Cranial osteology of the Early Cretaceous turtle *Pleurosternon bullockii* (Paracryptodira: Pleurosternidae) (#48267)

First submission

Guidance from your Editor

Please submit by **16 May 2020** for the benefit of the authors (and your $200 publishing discount) .

Structure and Criteria
Please read the 'Structure and Criteria' page for general guidance.

Author notes
Have you read the author notes on the guidance page?

Raw data check
Review the raw data.

Image check
Check that figures and images have not been inappropriately manipulated.

Privacy reminder: If uploading an annotated PDF, remove identifiable information to remain anonymous.

Files
Download and review all files from the materials page.

7 Figure file(s)

Structure and Criteria

Structure your review

The review form is divided into 5 sections. Please consider these when composing your review:

1. **BASIC REPORTING**
2. **EXPERIMENTAL DESIGN**
3. **VALIDITY OF THE FINDINGS**
4. General comments
5. Confidential notes to the editor

You can also annotate this PDF and upload it as part of your review

When ready submit online.

Editorial Criteria

Use these criteria points to structure your review. The full detailed editorial criteria is on your guidance page.

BASIC REPORTING

- Clear, unambiguous, professional English language used throughout.
- Intro & background to show context. Literature well referenced & relevant.
- Structure conforms to PeerJ standards, discipline norm, or improved for clarity.
- Figures are relevant, high quality, well labelled & described.
- Raw data supplied (see PeerJ policy).

EXPERIMENTAL DESIGN

- Original primary research within Scope of the journal.
- Research question well defined, relevant & meaningful. It is stated how the research fills an identified knowledge gap.
- Rigorous investigation performed to a high technical & ethical standard.
- Methods described with sufficient detail & information to replicate.

VALIDITY OF THE FINDINGS

- Impact and novelty not assessed. Negative/inconclusive results accepted. *Meaningful* replication encouraged where rationale & benefit to literature is clearly stated.
- All underlying data have been provided; they are robust, statistically sound, & controlled.
- Speculation is welcome, but should be identified as such.
- Conclusions are well stated, linked to original research question & limited to supporting results.

Standout reviewing tips

The best reviewers use these techniques

Tip	*Example*
Support criticisms with evidence from the text or from other sources	*Smith et al (J of Methodology, 2005, V3, pp 123) have shown that the analysis you use in Lines 241-250 is not the most appropriate for this situation. Please explain why you used this method.*
Give specific suggestions on how to improve the manuscript	*Your introduction needs more detail. I suggest that you improve the description at lines 57- 86 to provide more justification for your study (specifically, you should expand upon the knowledge gap being filled).*
Comment on language and grammar issues	*The English language should be improved to ensure that an international audience can clearly understand your text. Some examples where the language could be improved include lines 23, 77, 121, 128 – the current phrasing makes comprehension difficult.*
Organize by importance of the issues, and number your points	*1. Your most important issue* *2. The next most important item* *3. …* *4. The least important points*
Please provide constructive criticism, and avoid personal opinions	*I thank you for providing the raw data, however your supplemental files need more descriptive metadata identifiers to be useful to future readers. Although your results are compelling, the data analysis should be improved in the following ways: AA, BB, CC*
Comment on strengths (as well as weaknesses) of the manuscript	*I commend the authors for their extensive data set, compiled over many years of detailed fieldwork. In addition, the manuscript is clearly written in professional, unambiguous language. If there is a weakness, it is in the statistical analysis (as I have noted above) which should be improved upon before Acceptance.*

Cranial osteology of the Early Cretaceous turtle *Pleurosternon bullockii* (Paracryptodira: Pleurosternidae)

Serjoscha W Evers [Corresp., 1], **Yann Rollot** [1], **Walter G Joyce** [1]

[1] Department of Geosciences, University of Fribourg, Fribourg, Switzerland

Corresponding Author: Serjoscha W Evers
Email address: serjoscha.evers@googlemail.com

Pleurosternon bullockii is a turtle from the Early Cretaceous of Europe known from numerous postcranial remains. Only one skull has so far been referred to the species. *Pleurosternon bullockii* belongs to a group of turtles called pleurosternids, which is thought to include several poorly known taxa from the Late Jurassic and Early Cretaceous of Europe and North America. Pleurosternids and baenids, a group of North American turtles that lived from the Late Cretaceous to the Eocene, define a clade called Paracryptodira. Additionally, Paracryptodira likely includes compsemydids, and, potentially, helochelydrids. Character support for Paracryptodira is relatively weak, and many global phylogenetic studies fail to support paracryptodiran monophyly altogether. Proposed paracryptodiran synapomorphies are largely cranial, despite the poor characterization of pleurosternid cranial material. In addition to their questionable monophyly, the global position of paracryptodires is debated. Early studies suggest crown-turtle affinities, but most phylogenies find them as stem-turtles, irrespective of their monophyly. Here, we document the cranial osteology of *Pleurosternon bullockii* with the use of three-dimensional models derived from segmenting high-resolution X-ray micro-computed tomography (CT) scans. *Pleurosternon bullockii* has a primitive basipterygoid region of the skull, but a cryptodire-like acustico-jugular region. A surprising number of similarities with pleurodires exist, particularly in the laterally expanded external process of the pterygoid and in the posterior orbital wall. Our observations constitute an important step toward a phylogenetic re-evaluation of Paracryptodira.

Cranial osteology of the Early Cretaceous turtle *Pleurosternon bullockii* (Paracryptodira: Pleurosternidae)

Serjoscha W. Evers[1], Yann Rollot[1] and Walter G. Joyce[1]

[1]Department of Geosciences, University of Fribourg, Fribourg, Switzerland

Corresponding Author:

Serjoscha W. Evers[1]

Chemin de Musée 6, 1700 Fribourg, Switzerland

Email address: serjoscha.evers@unifr.ch

ABSTRACT

Pleurosternon bullockii is a turtle from the Early Cretaceous of Europe known from numerous postcranial remains. Only one skull has so far been referred to the species. *Pleurosternon bullockii* belongs to a group of turtles called pleurosternids, which is thought to include several poorly known taxa from the Late Jurassic and Early Cretaceous of Europe and North America. Pleurosternids and baenids, a group of North American turtles that lived from the Late Cretaceous to the Eocene, define a clade called Paracryptodira. Additionally, Paracryptodira likely includes compsemydids, and, potentially, helochelydrids. Character support for Paracryptodira is relatively weak, and many global phylogenetic studies fail to support paracryptodiran monophyly altogether. Proposed paracryptodiran synapomorphies are largely cranial, despite the poor characterization of pleurosternid cranial material. In addition to their

questionable monophyly, the global position of paracryptodires is debated. Early studies suggest crown-turtle affinities, but most phylogenies find them as stem-turtles, irrespective of their monophyly. Here, we document the cranial osteology of *Pleurosternon bullockii* with the use of three-dimensional models derived from segmenting high-resolution X-ray micro-computed tomography (CT) scans. *Pleurosternon bullockii* has a primitive basipterygoid region of the skull, but a cryptodire-like acustico-jugular region. A surprising number of similarities with pleurodires exist, particularly in the laterally expanded external process of the pterygoid and in the posterior orbital wall. Our observations constitute an important step toward a phylogenetic re-evaluation of Paracryptodira.

Key words: Testudines, Paracryptodira, Pleurosternidae, Baenidae, systematics, turtles

INTRODUCTION

Paracryptodires are often referred to as 'one of the three primary clades of (crown) turtles' (e.g. Joyce, 2017). This assessment is primarily based on unresolved phylogenetic positions between Pleurodira, Cryptodira, and Paracryptodira among early global phylogenetic studies (e.g. Joyce, 2007). However, most recent phylogenetic analyses recover paracryptodires as stem-turtles, just outside of the turtle crown (e.g. Sterli, 2010; Rabi et al., 2014; Cadena & Parham, 2015; Zhou & Rabi, 2015; Joyce et al., 2016; Evers & Benson, 2019). Paracryptodires were originally defined as a group of turtles that includes baenids, pleurosternids (including 'Glyptopsidae' of Gaffney, 1972), *Compsemys victa*, and *Kallokibotion bajazidi* (Gaffney, 1975a). Although only one formal phylogenetic analysis has since found these exact turtles in a monophyletic group (a Lyson & Joyce, 2011 analysis of the matrix of Gaffney et al., 2007), a sister relationship of

baenids with pleurosternids has been found frequently (e.g., Gaffney et al., 2007; Joyce, 2007; Lyson & Joyce, 2011; Pérez-García, Royo-Torres & Cobos, 2015; Joyce et al, 2016; Joyce & Rollot, in press). As a consequence, most authors associate the term 'Paracryptodira' with a clade that either exclusively includes baenids and pleurosternids (e.g. Joyce, 2007), or a clade that minimally includes these clades, variously joined by compsemydids, helochelydrids, or indeterminate paracryptodiran taxa (Lyson & Joyce, 2011). Lyson & Joyce (2011) formalized this notion of Paracryptodira by coining a stem-based phylogenetic definition that includes *Pleurosternon bullockii* and *Baena arenosa* as its internal specifiers. Character support for Paracryptodira is relatively weak. The main osteological feature that has historically been used to unite paracryptodires is a far anteriorly positioned foramen for the entry of the internal carotid artery (foramen posterius canalis carotici interni; Rabi et al., 2013) formed midway along the parabasisphenoid-pterygoid suture (Gaffney, 1975a). This feature persists to be cited as diagnostic for paracryptodires (see review of Joyce & Anquetin, 2019), although the foramen has repeatedly been interpreted to be absent altogether in at least in some paracryptodires (Sterli et al., 2010; Rabi et al., 2013; Anquetin & André, 2020). Additionally, many of the other originally proposed characters in support of the group are symplesiomorphically present in turtles (e.g. presence of nasal, reduced prefrontal exposure on skull roof, presence of mesoplastra, presence of paired gular scutes; Gaffney, 1975a). Some proposed synapomorphies, such as the reduction of the palatine artery (Gaffney, 1975a) or a reduced fenestra perilymphatica (Joyce, 2007), are, similar to the aforementioned position of the foramen posterius canalis carotici interni midway along the parabasisphenoid-pterygoid suture (Gaffney, 1975a; Joyce & Anquetin, 2019), not universally present in paracryptodires (e.g. Anquetin & André, 2020; this study) and should thus be re-evaluated on a broader scale. Ambiguity in character support of Paracryptodira is also

implicit from many global phylogenetic studies that fail to retrieve the clade as monophyletic altogether (Sterli, 2010; Anquetin, 2012; Sterli, Pol & Laurin, 2013; Cadena & Parham, 2015; Rabi et al., 2014; Zhou & Rabi, 2015; Joyce et al., 2016; Evers & Benson, 2019). Although most frequently cited paracryptodiran synapomorphies are cranial characters, non-baenid paracryptodiran skulls are poorly known (Joyce & Anquetin, 2019). Five taxa have relatively complete skulls, including the compsemydid *Compsemys victa* (Lyson & Joyce, 2011), the indeterminate paracryptodire *Uluops uluops* (Carpenter & Bakker, 1990), and the pleurosternids *Glyptops ornatus* (Gaffney, 1979a), *Dorsetochelys typocardium* (Evans & Kemp, 1976) and *Pleurosternon bullockii* (Evans & Kemp, 1975). Here, we re-examine UMZC T1041, the cranium of *Pleurosternon bullockii* that was originally described as *Mesochelys durlstonensis* by Evans & Kemp (1975), based on high-resolution micro-computed tomography (CT) scanning. We describe the cranium in detail and compare it to available material of other paracryptodires, and, where relevant, other groups of turtles. Thorough anatomical characterizations like the one presented here form the base work for phylogenetic assessments. Our description and comparisons provide anatomical evidence for unique morphologies of pleurosternids, which likely include at least *Uluops uluops* besides *Pleurosternon bullockii* and *Glyptops ornatus*. Pleurosternids show a mixture of plesiomorphic and derived features, tentatively supporting their inferred position as stem-taxa that are relatively close to the crown-node of turtles. We hope that our descriptions lead to the coding of novel phylogenetic characters, that further scrutinize the monophyly and global position of paracryptodires.

MATERIAL & METHODS

High-resolution X-ray computed tomography (CT) scans were obtained for the cranium of UMZC T1041, which is the holotype of *Mesochelys durlstonensis* Evans & Kemp, 1975. UMZC T1041 was found in the Early Cretaceous (Berriasian) Purbeck Limestone Group in Durlston Bay, United Kingdom (Evans & Kemp, 1975). Gaffney & Meylan (1988) referred the material to *Pleurosternon bullockii* Owen, 1842, albeit without justification. Milner (2004) compared the shell remains associated with the cranium of *Mesochelys durlstonensis* with those of *Pleurosternon bullockii*, and presented anatomical evidence for the synonymy suggested by Gaffney & Meylan (1988). This has generally been accepted ever since (see review of Joyce & Anquetin, 2019). Scans of UMZC T1041 were obtained by Roger Benson in 2017 at the Cambridge Biotomography Center, using a X-Tek H 225 μCT scanner (Nikon Metrology, Tring, UK). The cranium was scanned using a beam energy of 130 kV, a current of 250 μA, 500 ms exposure time, 1 frame per 1400 projections, and no filter, resulting in a voxel size of 0.03315 mm. The resulting CT-scans were segmented in the software Mimics (v. 16.0–19.0; http://biomedical.materialise.com/mimics), and 3D models were exported as .ply files. Figures of digital renderings were compiled using the software Blender v. 2.71 (blender.org). CT-slice data as well as the 3D models are deposited at MorphoSource (Evers, 2020).

We mostly compare UMZC T1041 to a selection of likely paracryptodires from the Late Jurassic to Cretaceous of North America and Europe based on description published in the literature, in particular *Arundelemys dardeni* (as described by Lipka et al., 2006), *Compsemys victa* (as described by Lyson & Joyce, 2011), *Dorsetochelys typocardium* (as described by Evans & Kemp, 1976 under the name *Dorsetochelys delairi*), *Eubaena cephalica* (as described by Rollot, Lyson & Joyce, 2018), *Glyptops ornatus* (as described by Gaffney, 1979a under the name *Glyptops plicatulus*), and *Uluops uluops* (as described by Carpenter & Bakker, 1990). For

115 comparisons with *Dorsetochelys typocardium*, we used a 3D model of the holotype (DORCM
116 G.00023) that was made available under a CC-BY-NC-SA license by the "GB3D Type Fossils"
117 projects hosted by the British Geological Survey at www.3d-fossils.ac.uk. The descriptions of
118 *Compsemys victa* (based on UCM 53971) and *Uluops uluops* (based on UCM 49223) were
119 complemented by CT scans of these specimens. The original descriptions are cited for all
120 previously described features, but the specimen numbers are cited when novel observations
121 regarding these taxa are made based on these scans. These scans will be further discussed and
122 made public in a forthcoming paper.
123
124 **DESCRIPTION**
125 **General comments.** The cranium of UMZC T1041 disarticulated into several blocks of fully to
126 partially articulated bones, which were then displaced to give the skull a crushed appearance
127 (Figs. 1, 2). The 3D anatomy of individual bones is nevertheless near perfect. For instance, the
128 left pterygoid, prootic, opisthotic, quadrate, and the parabasisphenoid form a block in which
129 these bones are still mostly preserved in their original positions relative to one another. The
130 parabasisphenoid, however, is shifted medially relative to the pterygoid.
131 The skull of UMZC T1041 is relatively low dorsoventrally, relatively narrow mediolaterally,
132 but elongate anteroposteriorly (Figs. 1, 2). The orbits face more laterally than in *Glyptops*
133 *ornatus* (Gaffney, 1979a), but less so than in *Compsemys victa* (Lyson & Joyce, 2011). The
134 entire skull roof and lateral side of the skull of UMZC T1041 is covered by the dense surface
135 sculpturing that is characteristic of many paracryptodires (e.g., Pérez-García, 2014; Joyce &
136 Lyson, 2015; Joyce & Anquetin, 2019). Although superficially the surface sculpturing of
137 paracryptodires is very similar among species, some differences can be made out. For instance,

138 although the main textural element in both *Uluops uluops* (Carpenter & Bakker, 1990; UCM
139 53971) and *Pleurosternon bullockii* (UMZC T1041) are small and irregular tubercles, these
140 transition into a ridge-like arrangement on the posterior margin of the parietal in UMZC T1042
141 (Fig. 2A), but not in *Uluops uluops* (UCM 53971). The skull emarginations of UMZC T1041 are
142 moderately developed: the cheek emargination is relatively deep, reaching about mid-orbit in
143 lateral view. The jugal and quadratojugal margins are strongly concave and the maxilla and
144 quadrate are included in the emargination (Fig. 2C–D). The same morphology is seen in *Uluops*
145 *uluops* (UCM 53971). The medial portion of the upper temporal emargination of UMZC T1042
146 is visible as a concavity developed along the posterior margin of the parietal that exposes only a
147 small part of the floor of the adductor chamber (Fig. 2A), again as in *Uluops uluops* (UCM
148 53971). The lateral portions of the upper temporal emargination that were likely formed by the
149 squamosal are damaged. Squamosal and supraoccipital crests are comparatively strongly
150 developed, providing elongate attachment sites for the adductor musculature.
151
152 **Nasal.** Only the left nasal of UMZC T1041 is preserved (Fig. 2A, C, E). However, as the left
153 nasal is in articulation with the frontal, prefrontal, and maxilla on the left side, the anterior region
154 of the skull roof can be completely reconstructed. The nasal is a triangular element that tapers
155 posteriorly and inserts into a gap between the prefrontal and frontal. The long anterior frontal
156 processes separate the paired nasals posteriorly, but anteriorly a short nasal-nasal suture can be
157 inferred, which is generally present in basal paracryptodires (Gaffney, 1972; Lyson & Joyce,
158 2015; Joyce & Anquetin, 2019).
159

Prefrontal. Both prefrontals of UMZC T1041 are preserved (Fig. 2). The prefrontal has a small skull roof exposure in UMZC T1041, and is restricted to a small area at the anterodorsal orbital margin, contacting the nasal, frontal, and maxilla. Evans & Kemp (1975) also reported a contact with the vomer. The relevant part of the specimen has since been lost, but the side of the descending process makes this contact highly plausible. Medially, the frontals hinder both prefrontals from a mutual contact. Anterolaterally, the prefrontal has a deep vertical groove for the reception of the ascending process of the maxilla, which is partially exposed on both sides due to partial disarticulation. However, on the left side, the maxilla and prefrontal are articulated enough to see that a small foramen orbito-nasale was laterally and dorsally framed by both bones. As the vomer and palatine bones are absent, the medial margin of the foramen is unknown. However, the foramen was medially probably closed by the palatine, as in *Uluops uluops* (UCM 53971).

Frontal. Both frontals are preserved (Fig. 2). The frontal contacts the nasal, prefrontal, postorbital, and parietal. The frontal is a relatively elongate, but narrow bone in UMZC T1041: the anterior portion forms long and narrow processes that divide the internasal contact for half of the nasal length (Fig. 2A). A process that partially separates the nasals is only slightly present in *Dorsetochelys typocardium* (Evans & Kemp, 1976) and *Arundelemys dardeni* (Lipka et al., 2006), but otherwise generally absent in other paracryptodires, such as *Glyptops ornatus* (Gaffney, 1979a), *Compsemys victa* (Lyson & Joyce, 2011), or baenids (Gaffney,1972; Joyce & Lyson, 2015). The frontal contributes to the orbit in UMZC T1041 by means of a broad lateral process (Fig. 2A). Ventrally, both frontals form a narrow sulcus olfactorius that extends

anteriorly into the fossa nasalis (Fig. 3). The right and left crista cranii diverge posteriorly from the midline and become shallower near the suture with the parietal.

Parietal. Both parietals are preserved in UMZC T1041 (Fig. 2). The parietal forms the posterior and central parts of the skull roof and contacts the frontal anteriorly, the postorbital laterally, and almost certainly the squamosal posterolaterally. Ventrally, the parietal contacts the supraoccipital, prootic, epipterygoid, and possibly the pterygoid (Fig. 4B). The parietal forms a tapering posteromedian process, which seems to have covered the supraoccipital entirely (see supraoccipital). The posterior margin of the parietal is emarginated lateral to the midline, but still conceals most of the otic capsule in dorsal view (Fig. 2A), as is also the case in *Dorsetochelys typocardium* (Evans & Kemp, 1976) and *Uluops uluops* (UCM 53971). The right parietal of UMZC T1041 is broken posterolaterally near the squamosal, so that the contact between these bones is not preserved. However, if the right squamosal were a mirror image of the one on the left side, where the squamosal is missing but the parietal completely preserved, both bones would clearly have a short contact posterior to the postorbital, as is also the case in *Dorsetochelys typocardium* (Evans & Kemp, 1976) and *Uluops uluops* (UCM 53971).

The descending process of the parietal is well-developed in UMZC T1041 (Figs. 3, 4B), although the anterior margin of the process is posteriorly retracted, so that the interorbital fenestra is large. Internally, the medial surface of the base of the descending process seems bulged within the endocranial cavity, suggesting that *Pleurosternon bullockii* possibly had large cerebral hemispheres. The posteroventral margin of the descending process of the parietal contacts the supraoccipital posteriorly and the prootic anteriorly. At the dorsal margin of the trigeminal foramen, the parietal forms a thin posteroventral process that also frames the posterior

margin of the foramen, and extends to contact the pterygoid, thereby excluding the prootic from contributing to the foramen (Fig. 4). This is visible on the right side of UMZC T1041, where the prootic, parietal, quadrate, and partially the pterygoid and epipterygoid are preserved in articulation. The same arrangement can be observed in *Uluops uluops* (UCM 53971) at the posterior margin of the trigeminal foramen. A posteroventral process of the parietal along the posterior trigeminal foramen margin has been proposed as a synapomorphy of Thalassochelydia (Anquetin, Püntener & Joyce, 2017), based on the presence of this process in *Solnhofia parsonsi* and plesiochelyids (Anquetin, Püntener & Billon-Bruyat, 2015). The same process has also been observed in sandownids (Evers & Joyce, 2020). The presence of this process in paracryptodires as well as the aforementioned groups, all of which have recently been interpreted as stem-turtles (e.g. Evers & Benson, 2019), indicates that this could be a feature that is more widespread along the crownward stem-lineage of turtles. The contacts of the parietal of UMZC T1041 anteroventral to the trigeminal foramen are not clearly preserved on either side of the specimen. However, contacts with both the epipterygoid and pterygoid were likely present.

Most of the lateral contact with the postorbital is formed as a simple, planar contact without further reinforcement. However, at the level of the base of the descending process, the parietal expands laterally underneath the postorbital (Fig. 3). The ventral surface of this buttress is hypertrophied to a mediolateral ridge between the descending process of the parietal and the ventral process of the postorbital. This shallow ridge forms the posterior boundary of a shallow fossa that is anteriorly bound by the medial margin of the orbital fossa, and which we identify as as the roof to the sulcus palatino-pterygoideus (see postorbital). The same fossa is also present in various other turtle, though rarely reported, we note that it is particularly deep in UMZC T1041, *Uluops uluops* (UCM 53971), and pleurodires (Gaffney, Tong, & Meylan, 2006).

228

229 **Postorbital.** Both postorbitals are preserved in UMZC T1041 (Fig. 2). The postorbital contacts
230 the frontal anteromedially, the parietal posteromedially, the squamosal posteriorly, the
231 quadratojugal posteroventrally, and the jugal ventrally.

232 The postorbital of UMZC T1041 is posteriorly elongate (Fig. 2A–D) and forms the extensive
233 temporal roofing together with the parietal. However, the postorbital is excluded from the
234 posterior margin of the skull roof by a squamosal-parietal contact. The postorbital and squamosal
235 contact is located dorsal to the margin of the cavum tympani, but separated from contacting the
236 cavum or quadrate by a posterior process of the quadratojugal (Fig. 2D). The quadratojugal
237 contacts the postorbital posterior to the jugal-postorbital contact.

238 The postorbital forms the posterior margin of the orbit (Fig. 2C–D). Although the preservation
239 of UMZC T1041 leaves a bit of room for interpretation regarding the posterior orbital margin, it
240 seems that the jugal was excluded clearly from contributing to the margin of the orbit by a short
241 ventral process of the postorbital that contacted the maxilla (see jugal). Within the orbital fossa,
242 the postorbital forms an expanded ventral process that contacts the medial process of the jugal
243 ventrally (Fig. 3). Hereby, the ventral process of the postorbital nearly contacts the pterygoid,
244 and a contact with the unpreserved palatine cannot be ruled out entirely. The morphology of the
245 ventral process of the postorbital seems to be very similar in *Uluops uluops* (UCM 53971). In
246 this taxon, the postorbital comes close to the pterygoid and palatine, but both contacts are absent.
247 A postorbital-palatine contact is only seen in pleurodires (Gaffney, 1979b). However, the orbito-
248 temporal region of both UMZC T1041 and *Uluops uluops* (UCM 53971) show striking
249 similarities to the morphology of that region in pleurodires: the medial postorbital-jugal
250 expansion forms an extended posterior wall to the orbital fossa (Fig. 3). Additionally, again as in

pleurodires, the passage between the temporal fossa posteriorly, and the orbital fossa anteriorly, becomes strongly constricted between the ventral process of the postorbital and the descending process of the parietal (Fig. 3). Furthermore, the roof of this constricted through is depressed to form a shallow fossa (Fig. 3). This morphology is otherwise only found in pleurodires (e.g. Gaffney, Tong & Meylan, 2006). Thus, we use terms from the pleurodire literature to refer to these respective structures; we use 'septum orbitotemporale' for the medial expanded jugal-postorbital wall (Gaffney, Tong & Meylan, 2006: fig. 25), and we use 'sulcus palatino-pterygoideus' for the space between the orbital and temporal fossae (Gaffney, Tong & Meylan, 2006: fig. 25), although we note that it is incipient with respect to the pleurodire morphology. Another potential similarity of UMZC T1041 with pleurodires is the spatial relationship between the foramen palatinum posterius and the septum orbitotemporale. Although not completely preserved, the foramen palatinum posterius of UMZC T1041 seems to be located posteriorly to the level of the septum orbitotemporale, as in all pleurodires, but also an eclectic group of cryptodires. The foramen palatinum posterius of *Uluops uluops* (UCM 53971) is positioned anterior to the septum orbitotemporale.

Jugal. Both jugals of UMZC T1041 are preserved (Fig. 2A–D), but the elements are disarticulated slightly from their surrounding bones. Definite contacts are with the postorbital, maxilla, quadratojugal, and pterygoid, and a contact with the palatine cannot be ruled out. The jugal of UMZC T1041 shows typical turtle morphology with a laterally placed, vertical plate that forms part of the lateral skull roof, and a medially directed process that contacts parts of the palate. The jugal is removed from the ventral skull margin, as the maxilla forms a posterior process that extends ventrally underneath the jugal for some distance (Fig. 2C–D). The end of

this maxillary process forms the beginning of the moderately deep lower temporal skull emargination, which extends from the maxilla along the ventral margins of the jugal and quadratojugal. The dorsally positioned jugal and step-like margin between the maxilla and jugal are also present in *Uluops uluops* (UCM 53971), *Glyptops ornatus* (Gaffney, 1979a), and baenids (Gaffney, 1972), but not so in *Dorsetochelys typocardium* (Evans & Kemp, 1976), in which the jugal is the posterior continuation of the maxilla along the labial margin of the skull.

It seems that the jugal was excluded from the orbital margin, as is also the case in *Glyptops ornatus* (Gaffney, 1979a), *Arundelemys dardeni* (Lipka et al., 2006), and an assortment of advanced baenids (Gaffney, 1972; Joyce & Lyson, 2015; Rollot, Lyson & Joyce, 2018) as well as helochelydrids (e.g. Joyce et al., 2011; Joyce, Sterli & Chapman, 2014): on both sides, the jugal of UMZC T1041 has an anteriorly recessed surface, which is posteriorly delimited by a rim. Only posteriorly to this rim does the surface of the bones show the sculpturing that covers most of the external bone surfaces (Fig. 2C–D). In *Uluops uluops* (UCM 53971), in which the jugal contributes to the orbit, the surface sculpturing of the jugal bone indeed extends to the orbit. Thus, we interpret the recessed surface in UMZC T1041 to be a laterally exposed facet for the overlying postorbital and maxilla. Our interpretation hereby differs markedly from that of Evans & Kemp (1975), who reconstructed a point contact of the jugal to the orbit margin. Despite its likely exclusion from the orbital margin itself, the jugal of UMZC T1041 is expressed medially to the orbital margin within the orbital fossa, which we call septum orbitotemporale (see postorbital) (Fig. 3). Extending posteromedially from the orbital fossa, the medial process of the jugal reaches the pterygoid. This section of the jugal is ventrally overlain by the maxilla. A contact with the palatine might have been present in this area, but this cannot be confirmed without any indication of the morphology of the palatine bone.

297

298 **Quadratojugal.** The quadratojugal is only preserved on the right side of UMZC T1041 (Fig.
299 2D). The quadratojugal is triradiate, as it forms a posterior process that inserts between the
300 postorbital and quadrate to contact the squamosal, extends ventrally along the anterior quadrate
301 margin, and anteriorly towards the jugal. The quadratojugal of *Pleurosternon bullockii* is a
302 comparatively small bone in comparison to those of basal stem-turtles (e.g., Gaffney, 1990) or
303 baenids (e.g., Joyce and Lyson, 2015; Rollot, Lyson & Joyce, 2018), but not as small as in
304 sichuanchelyids (Sukhanov, 2000; Joyce et al., 2016), which have quadratojugals with a greatly
305 reduced lateral exposure. The quadratojugal of UMZC T1041 is similar in size and extent to that
306 of *Uluops uluops* (UCM 53971). In UMZC T1041, the ventral margin of the quadratojugal
307 contributes to the moderately deep lower temporal emargination. Although the quadratojugal
308 frames the quadrate anteriorly, it is slightly displaced anteriorly from the margin of the cavum
309 tympani, and clearly does not closely approach the articular condyles of the quadrate.

310

311 **Squamosal.** Only the right squamosal of UMZC T1041 is preserved (Fig. 2). Contacts with the
312 quadratojugal, quadrate, and opisthotic can be documented, and a parietal contact is inferred. The
313 squamosal of *Pleurosternon bullockii* is a large element with a well-developed posterior process
314 and a deeply recessed antrum postoticum. The squamosal caps the posterior part of the quadrate,
315 and hereby forms the posterodorsal margin of the deeply developed cavum tympani, as is also
316 the case in *Uluops uluops* (UCM 53971) and baenids (Joyce & Lyson, 2015). The squamosal of
317 UMZC T1041 has a deep, incision-like facet for the opisthotic, and thus frames the paroccipital
318 process from dorsal and ventral. Whereas the anterior part of the squamosal is bulbous and
319 houses the expanded antrum postoticum, the bone narrows mediolaterally toward its posterior

end to form a vertically sheeted process that extends posteriorly just beyond the level of the supraoccipital crest (Fig. 2A, F).

Premaxilla. Both premaxillae are preserved in UMZC T1041, although the left one is broken into two pieces that are attached to different blocks (Fig. 2A–E). The premaxilla contacts the maxilla, but contacts with the palatine are uncertain due to incomplete preservation. A contact with the vomer was originally preserved (Evans & Kemp, 1975), but the vomer is now lost (see vomer). The right premaxilla completely surrounds a clearly developed foramen praepalatinum (Fig. 2B), which is only incompletely preserved on the other side. The dorsal margin of the premaxilla shows that the external naris was undivided from below in *Pleurosternon bullockii*, as described by Evans & Kemp (1975). Within the nasal fossa, both premaxillae together form a low ridge that probably serves as the insertion for the internarial septum. The full labial ridge, including the premaxillae, frame a broad notch along the midline. Serrations on the premaxillary labial ridge, as reported by Evans and Kemp (1975), are not confirmed for UMZC T1041.

Maxilla. Both maxillae are preserved in UMZC T1041 (Fig. 2A–E). The maxilla contacts the premaxilla anteriorly, the nasal and prefrontal dorsally, the jugal and postorbital posteriorly, and the pterygoid posteromedially. A medial contact with the vomer was previously documented by Evans & Kemp (1975), but is not preserved anymore. A contact with the palatine was likely present along the medial margin of the triturating surface. The triturating surface of the maxilla is relatively narrow and lacks a medial ridge (Fig. 2B). The labial ridge is ventrally deep and sharp-edged (Fig. 2B). In anterior view, the labial ridge of the maxilla and premaxilla jointly frame a broad, but shallow median notch (Fig. 2E). A curved labial margin of the maxilla seems common

among paracryptodires, although the degree of the curvature varies. UMZC T1041 is intermediate in this regard between *Glyptops ornatus* (Gaffney, 1979a), *Dorsetochelys typocardium* (Evans & Kemp, 1976), and *Arundelemys dardeni* (Lipka et al., 2006) with a weakly curved maxilla on one side, and *Uluops uluops* (UCM 53971) on the other, in which the curvature is very strongly pronounced. The medial margin of the incompletely preserved foramen orbito-nasale of UMZC T1041 is formed by the maxilla, and the foramen alveolaris superior is a comparatively large foramen positioned within that margin (best viewed in the 3D models). Posterior to the ascending process, the maxilla forms the complete ventral margin of the orbit (Fig. 2C–D). The margin is slightly raised to an orbital rim, medial to which the maxilla forms a narrow floor of the orbital fossa. The foramen supramaxillare is small and positioned immediately anterior to the jugal contact within the floor of the orbital fossa (Evans & Kemp, 1975). Posteriorly, the maxilla laterally overlaps the jugal to contact the postorbital along the posterior margin of the orbit (see jugal). The maxilla also extends ventrally to the jugal with a short process (Fig. 2C–D). The posterior part of the maxilla is medially expanded underneath the jugal and reaches the anterior end of the external process of the pterygoid.

Vomer. Evans & Kemp (1975) describe and illustrate a small anterior part of the vomer that was articulated with the premaxillae and the prefrontals. However, this part of the vomer, alongside a small posterior part of the left premaxilla is not preserved in the specimen anymore, and the whereabout of the fragments that must have broken off since the description of Evans & Kemp (1975) are unclear.

Palatine. The palatines are not preserved in UMZC T1041.

366

367 **Quadrate.** Both quadrates of UMZC T1041 are preserved (Fig. 2B–D, F). The quadrate contacts
368 the prootic and opisthotic medially, the pterygoid anteroventrally, the epipterygoid anteriorly, the
369 quadratojugal anterolaterally, and the squamosal posterolaterally. A point contact with the
370 supraoccipital is likely just posterior to the foramen stapedio-temporale. The lateral surface of
371 the quadrate is dominated by the deeply recessed cavity that forms most of the cavum tympani
372 (Fig. 2C–D). The quadrate forms the anterior margin of the cavum tympani, but posterolaterally
373 this structure is formed by the squamosal. The incisura columella auris is posteroventrally open,
374 as in all other paracryptodires (Joyce & Lyson, 2015; Joyce & Anquetin, 2019). The articular
375 process of the quadrate of UMZC T1041 does not protrude ventrally very deep and does not
376 significantly expand beyond the ventral margin of the cavum tympani. Much of the lateral
377 surface of the articular process was probably covered by the ventral ramus of the quadratojugal.
378 In ventral view, the articular surface of the process bears two weakly convex sub-facets (Fig.
379 2B), which are mediolaterally separated by a shallow sulcus (Evans & Kemp, 1975). The medial
380 side of the articular process is buttressed by the posterior process of the pterygoid, but the
381 process does not reach the articular facet (Fig. 2B). Medially, within the cavum acustico-
382 jugulare, the quadrate forms together with the pterygoid and prootic the posterior foramen for the
383 canalis cavernosus. Between the prootic and quadrate, the canalis stapedio-temporalis connects
384 the cavum acustico-jugulare with the adductor chamber (Fig. 5A). The respective exiting
385 foramen, the foramen stapedio-temporale, is formed on the dorsal surface of the otic capsule at
386 the posterior limit of the contact between the quadrate and prootic (Fig. 4A). Immediately
387 posterior to the foramen, the quadrate likely has a short, superficial contact with the
388 supraoccipital, which can also be observed in *Uluops uluops* (UCM 53971) and some baenids

like *Stygiochelys estesi* (Gaffney, 1972). Contacts of the quadrate with the opisthotic and squamosal form the posterior aspect of the floor of the adductor chamber in UMZC T1041. Anteriorly within the adductor chamber, the dorsal surface of the quadrate contributes to the formation of the weakly developed processus trochlearis oticum. However, the quadrate forms less of the process than the prootic. The process is developed as a shallowly concave area along the quadrate-prootic contact (Fig. 4A). The processus trochlearis oticum of *Uluops uluops* (UCM 53971) is somewhat more pronounced, but otherwise similar to that of *Pleurosternon bullockii*. The anterior quadrate surface of UMZC T1041, ventral to the processus trochlearis oticum, extends anteriorly in a short epipterygoid process (Fig. 4A). This process contacts the epipterygoid but is excluded from the trigeminal foramen margin by a dorsal process of the pterygoid.

Epipterygoid. In UMZC T1041, we identify a small plate-like ossification ventral to the trigeminal foramen as the epipterygoid and thus agree with Evans & Kemp (1975) in the identification of this element. However, the epipterygoids are difficult to segment in our CT scans, due to their highly interdigitated sutures with the parietals, and fragmentation due to breakage in the respective skull area. On the right side of the specimen, the epipterygoid seems to be preserved close to its original position, although its dorsal margin has tipped laterally (Fig. 4). Here, the epipterygoid is positioned anteriorly to the epipterygoid process of the quadrate and ventrally to the descending process of the parietal. If the epipterygoid were tilted back into contact with the parietal, it would frame the anteroventral margin of the trigeminal foramen, its usual position (e.g., Gaffney, 1979b). The left epipterygoid, which seems to have been misplaced slightly dorsally, also indicates that a contact with the prootic is likely.

412

413 **Pterygoid.** Both pterygoids of UMZC T1041 are preserved (Fig. 2B). The right pterygoid is
414 basically complete (Fig. 6), but has a transverse break through its center, whereas in the left
415 pterygoid, the external process is broken off but preserved. The pterygoid contacts the
416 parabasisphenoid, jugal, maxilla, parietal, epipterygoid, quadrate, prootic, opisthotic. Although
417 the palatines and the basioccipital are absent, contacts with the pterygoid seem all but certain.
418 However, as the exoccipitals are missing as well, we cannot assess if a pterygoid contact was
419 present with this bone as well. An interpterygoid contact below the rostrum basisphenoidale is
420 certainly absent (see Parabasisphenoid), but a possible midline contact anterior to the
421 parabasisphenoid cannot be ruled out, as the anterior tips of the pterygoids might be damaged.
422 The pterygoid of *Pleurosternon bullockii* shows a mixture of primitive and advanced features,
423 as well as similarities to pleurodires and cryptodires. The general architecture of the bone mimics
424 that of most cryptodires, with a relatively long posterior process that covers large parts of the
425 cavum acustico-jugulare from ventral exposure (Figs. 2B, 5A). The posterior process extends
426 posteriorly up to the tips of the posterior parabasisphenoid processes (= anterior tubercula
427 basioccipitale; see parabasisphenoid), and certainly contacted the basioccipital, as is also the case
428 in *Uluops uluops* (UCM 53971). The posterior pterygoid process of UMZC T1041 furthermore
429 completely covers the ventral end of the processus interfenestralis of the opisthotic (Fig. 2B,
430 5A), as in *Uluops uluops* (UCM 53971) and *Glyptops ornatus* (Gaffney, 1979a). Thus, the
431 process is much more cryptodire-like and extensive than acknowledged in previous descriptions
432 (Evans & Kemp, 1975), although Gaffney (1979a) corrected earlier statements of his, and also
433 argued that in both *Glyptops ornatus* and UMZC T1041 the posterior process of the pterygoid is
434 indistinguishable from cryptodires. Between the articular process of the quadrate and the

parabasisphenoid of UMZC T1041, the posterior process of the pterygoid shows a well-developed pterygoid fossa (Figs. 6A, 7C). Despite this cryptodire-like appearance, the pterygoid retains a deep, pocket-like facet on its medial margin for the reception of the basipterygoid processes of the parabasisphenoid (Figs. 6A, 7C). This facet is absent in the crania of all Recent turtles. The medial margin of the pterygoid is laterally curved around the basipterygoid articulation, which results in the formation of a window-like recess in the floor of the basicranium, through which the basipterygoid process of the parabasisphenoid is partially exposed, and through which the cerebral artery and the vidian nerve enter the cranium. The articulation socket for the basipterygoid process within the medial surface of the pterygoid bears a central foramen, which is positioned between the dorsal and ventral flanges of the basipterygoid process (see Parabasisphenoid). The foramen is the entry to the canalis nervus vidianus, which transmits the vidian nerve through the pterygoid towards an anterior foramen that is positioned lateral to the anterior end of the crista pterygoidei (Fig. 6B). The connection of these two foramina and their identification as the canalis nervus vidianus were already correctly inferred by Evans & Kemp (1975), but the foramen within the basipterygoid facet was re-interpreted by Sterli et al. (2010) as the posterior entry foramen of the palatine artery. Our CT scans unambiguously confirm the internal connection of the above-mentioned foramen with the anterior foramen of the canalis nervus vidianus, and thus corroborate the interpretation by Evans & Kemp (1975). Gaffney (1979a) described the presence of a palatine artery canal for *Glyptops ornatus* that extends anteriorly from within the basipterygoid articulation socket of the pterygoid, but he could not find an anterior exiting foramen. Thus, it is possible that Gaffney (1979a) misinterpreted the foramen he saw, which could instead be for the vidian nerve canal, and did not find an anterior palatine artery canal foramen, because it does not exist. However, this can only

458 be tested with certainty by attaining CT scans of *Glyptops ornatus*. For UMZC T1041, we can
459 furthermore confirm the canalis pro ramo nervi vidiani of Evans & Kemp (1975; foramen pro
460 ramo nervi vidiani prior to revision of Rollot, Lyson & Joyce [2018]), as a vertically oriented
461 canal that extends through the pterygoid from the floor of the canalis cavernosus to the ventral
462 pterygoid surface posterior to the parabasisphenoid articulation (Fig. 7C). The canalis pro ramo
463 nervi vidiani seems to be present in the same location in *Glyptops ornatus* (Gaffney, 1979a).
464 Immediately anterior to the ventral opening of the canalis pro ramo nervi vidiani of UMZC
465 T1041, a robust ridge surrounds the ventromedial margin of the pterygoid around the
466 basipterygoid facet (Evans & Kemp, 1975). Both the ventral canalis pro ramo nervi vidiani and
467 the robust ridge are affected by the large break of the right pterygoid, but nicely preserved on the
468 left element (Fig. 7C). The ridge persists anteriorly, albeit much more shallowly, parallels the
469 parabasisphenoid suture for a short distance, and curves laterally toward the posteriorly directed
470 tip of the external pterygoid process (Fig. 6A). Evans & Kemp (1975) interpret the ridge to be
471 the insertion for the pterygoideus musculature, and the same ridge morphology is present in
472 *Glyptops ornatus* (Gaffney, 1979a). In *Uluops uluops* (UCM 53971), the pterygoideus muscle
473 ridge is similar, but the ridge traverses the pterygoid earlier and extends to the posterior end of
474 the external process, thus defining a smaller fossa.
475 The external process of the pterygoid is extremely large in UMZC T1041 and projects
476 laterally deeply into the subtemporal fenestra (Figs. 2B, 5A–B, 6). Although many turtles,
477 including many cryptodires, have their lateral surface of the external process developed to a
478 vertical flange, this morphology seems hypertrophied in *Pleurosternon bullockii*. The vertical
479 plate of the lateral surface of the external process is less sheeted than in most cryptodires that
480 have the respective flange, but is more robust, and notably gently medially deflected towards its

dorsal margin (Fig. 6B–C, 5A–B, 4). As such, the morphology of the external process of the pterygoid of UMZC T1041 comes very close to that of a pleurodiran processus trochlearis pterygoidei. Additionally, although the external process of the pterygoid is anteriorly sutured to the jugular-maxillar area in many turtles, including some cryptodires and early stem turtles like *Proganochelys quenstedtii* (e.g. Gaffney, 1990), the deep and large facet for the articulation with the jugal (Fig. 6B–C, 4) demonstrates an unusually strong structural integration of the external process into the mechanical framework of the cranium, as is also seen in many pleurodires. However, the lateral surface of the external process is parallel to the skull midline (Fig. 2B), and the process is not laterally tilted with its posterior end, as is the case in pleurodiran pterygoid trochleae. As such, the trajectory of the adductor muscles, when approximated around the weak otic trochlea present on the prootic of UMZC T1041, do not seem to be guided around the external process. As the detailed morphology of the external process is rarely described in detail, we cannot exclude the possibility that this morphology is perhaps wider spread that noted herein.

The dorsal surface of the pterygoid of UMZC T1041 is curved around the anteriorly narrowing parabasisphenoid. Posteriorly, the medial part of the dorsal surface is dominated by a low buttress for articulation with the prootic and parabasisphenoid, which also forms the medial wall of the canalis cavernosus (Fig. 6B–C). The lateral surface of this canal is formed by the crista pterygoidei. The canalis cavernosus ends anteriorly in the foramen cavernosum formed between the prootic and pterygoid. Anterior to the foramen, the canalis cavernosus continues as the sulcus cavernosus and parallels the rostrum basisphenoidale of the parabasisphenoid (Fig. 6B–C). At the anterior end of the crista pterygoidei, there is a small exiting foramen for the canalis nervus vidianus (Evans & Kemp, 1975; Fig. 6B–C). The crista pterygoidei itself is relatively low and posteriorly interrupted by a deep notch for the trigeminal foramen. In the

posterior margin of this foramen, the pterygoid extends dorsally to reach the parietal and thus excludes the prootic from contributing to the foramen (Fig. 4B). The same dorsal process is present in *Uluops uluops* (UCM 53971). The crista pterygoidei of UMZC T1041 is laterally overlapped by the epipterygoid anterior to the trigeminal foramen (Fig. 4B).

Supraoccipital. The supraoccipital of UMZC T1041 is nearly completely preserved. It ventrolaterally contacts the prootic and opisthotic and perhaps has a point contact with the quadrate (Figs. 2, 4). It furthermore contacts the parietal anteroventrally and dorsally, and likely contacted the exoccipital posteroventrally.

The supraoccipital of UMZC T1041 forms a comparatively broadly arched roof to the endocranial cavity (Fig. 2F). A vertical plate extends over the entire anteroposterior length of the supraoccipital, but this plate does not seem to extend posteriorly from the approximate position of the foramen magnum as a supraoccipital crest (Evans & Kemp, 1975). This crest seems dorsally nearly completely covered by the parietals. The supraoccipital was likely only marginally visible in the skull roof between the parietals, though much less than interpreted by Evans & Kemp (1975). This differs from the conditions in *Uluops uluops* (UCM 53971), *Glyptops ornatus* (Gaffney, 1979a), and *Dorsetochelys typocardium* (Evans & Kemp, 1976), in which the supraoccipital crest is topped by a triangular or diamond shaped horizontal plate that forms a marginal part of the dorsal skull roof. Within the otic capsule of UMZC T1041, the supraoccipital articulates with the prootic anteriorly and the opisthotic posteriorly. Between both bones, the supraoccipital likely extends laterally to have a small superficial contact with the quadrate, as is also the case in *Uluops uluops* (UCM 53971). The hiatus acusticus of UMZC T1041 is a large, unossified space between the supraoccipital, prootic, parabasisphenoid, and

opisthotic, leaving a large opening between the inner ear cavity and the endocranial cavity. Dorsally above the hiatus acusticus, the foramen aquaducti vestibuli, i.e. the canal for the endolymphatic duct, is completely embedded within bone, forming a short canal from the endocranial cavity into the recess of the supraoccipital that holds the common crus of the labyrinth. Evans & Kemp (1975) reported that the foramen aquaducti vestibuli is only a notch in the supraoccipital margin, but as completely ossified canals exist on both sides of the supraoccipital, they probably misinterpreted a small break on the left side of the element and missed the small foramina. Contacts with the lost exoccipitals can be inferred from short facets posterior to the articulation site for the opisthotic.

Exoccipital. The exoccipitals are not preserved in UMZC T1041.

Basioccipital. The basioccipital is not preserved in UMZC T1041.

Prootic. Both prootics of UMZC T1041 are present, but the right one is better preserved. The prootic has a large exposure within the floor of the adductor chamber, forming the anteromedial part of the otic capsule (Fig. 4). Its dorsal surface is transversely concave and anteroventrally sloping toward the subtemporal fossa (Fig. 4A). Although this surface does not protrude anteriorly into the fossa, this morphology clearly indicates a redirecting of the jaw adductor musculature. Thus, a small processus trochlearis oticum is present. A very similar morphology, although more pronounced by a deeper concave flexure across the prootic, is seen in *Uluops uluops* (UCM 53971). Anteroventrally, the prootic of UMZC T1041 forms the dorsal margin of the foramen cavernosus. Slightly anterodorsally to the position of this foramen, the prootic is

550 slightly expanded transversely to form the posterior wall of the fossa epiptericum for the
551 trigeminal ganglion. However, the anteroventral margin of the prootic is excluded from the
552 trigeminal foramen itself, contra the description of Evans & Kemp (1975; Fig. 4B).
553 Medioventrally, the prootic has a large, foot-like process that contacts the pterygoid and
554 parabasisphenoid. The medial surface of this ventral prootic process is recessed by the fossa
555 acustico-facialis, from which the facial nerve canal extends through the ventral prootic process
556 toward the canalis cavernosus, and from which the short acustic nerve canals lead into the
557 prootic part of the cavum labyrinthicum. This cavity for the labyrinth deeply excavates the
558 prootic from posterior (Fig. 5A–B). The canal for the lateral semicircular duct of the labyrinth
559 organ is already ossified within the prootic, and thus shared between prootic and opisthotic (Fig.
560 5B, D). Ventrally, a horizontal footplate of the ventral prootic process extends posteriorly and
561 floors the anterior half of the cavum labyrinthicum (Fig. 5). This footplate contacts the opisthotic
562 across the entire transverse width of the cavum labyrinthicum, so that the fenestra ovalis is
563 completely surrounded, dorsally and ventrally, by these two bones (Fig. 5C–D). The same
564 condition is present in *Uluops uluops* (UCM 53971) and *Glyptops ornatus* (Gaffney, 1979a).
565 Laterally to the fenestra ovalis of UMZC T1041, and thus within the cavum acustico-jugulare,
566 the posteriorly exposed surface of the prootic is deeply recessed by a fossa (Fig. 5B–C), which
567 has been hypothesized to be related to the perilymphatic system of reentrant fluid-flow systems
568 in turtle ears (e.g. Evers & Benson, 2019; Evers et al., 2019; Foth et al., 2019), and which is also
569 present in *Uluops uluops* (UCM 53971). Because the fossa continues dorsolateral to the fenestra
570 ovalis onto the opisthotic, we use the term perilymphatic fossa instead of posterior prootic recess
571 as in some previous works (e.g. Evers & Joyce, 2020). Laterally to the perilymphatic fossa, the
572 pterygoid and prootic form the posterior foramen for the canalis cavernosus. The mediodorsal

573 wall of the canalis cavernosus, formed by the prootic, is incised by a sulcus for the
574 hyomandibular nerve (Fig. 5B), which extends from the lateral foramen of the facial nerve canal
575 to the posterior foramen for the canalis cavernosus. Such a sulcus is also present in *Uluops*
576 *uluops* (UCM 53971).
577
578 **Opisthotic.** The opisthotics are nearly completely preserved on both sides of the cranium of
579 UMZC T1041, but while the left one remains in articulation with the adjacent prootic and
580 quadrate on the left side, the right one is ventrally displaced (Figs. 2B, F, 5C–D). The opisthotic
581 contacts the prootic anteriorly, the supraoccipital medially, the exoccipital
582 posteroventromedially, the parabasisphenoid ventrally, the quadrate and squamosal laterally, and
583 the pterygoid ventrally.
584 The anterior part of the opisthotic forms parts of the cavum labyrinthicum (Fig. 5C–D). On
585 the right opisthotic, the processus interfenestralis, which walls the cavum labyrinthicum
586 posteriorly, is broken off (Fig. 5A). On the left element, the process is also damaged, but still
587 preserved in articulation with the underlying pterygoid (Fig. 5C–D). The processus
588 interfenestralis is delicate in UMZC T1041, but resembles the process of mesochelydians by
589 reaching ventrally to fully separate the cavum labyrinthicum from the recessus scalae tympani.
590 At the dorsal base of the processus interfenestralis, the lateral foramen for the glossopharyngeal
591 nerve is visible (Fig. 5A, C). The ventral end of the process is expanded to a small footplate that
592 articulates with the dorsal surface of the pterygoid, and frames the fenestra ovalis
593 posteroventrally (Fig. 5C–D). The footplate of the process also minimally contacts the
594 parabasisphenoid, which has a dorsally high margin surrounding the ‘cup’ that holds parts of the
595 brain. The processus interfenestralis is centrally broken on the left side of UMZC T1041,

probably where the foramen perilymphatica minimized its structural integrity. Whereas the ventral part with the footplate is in perfect articulation with the prootic and pterygoid, the dorsal part of the process and the remainder of the left opisthotic are slightly misplaced with regard to their original position. Although the fenestra perilymphatica is thus collapsed, there is no reason to believe its size was smaller than that of other turtles, as sometimes stated for paracryptodires and *Pleurosternon bullockii* specifically (e.g. Brinkman & Nicholls, 1993; Gaffney, 1996; Joyce, 2007). Additionally, the perilymphatic foramen of *Uluops uluops* (UCM 53971) is of 'regular' size, and the morphology of the processus interfenestralis of this taxon is very similar to that of *Pleurosternon bullockii*. Laterally and slightly anteriorly to the base of the processus interfenestralis of UMZC T1041, there is a shallow sulcus in the roof of the cavum acustico-jugulare, the perilymphatic fossa, which continues anteriorly to become confluent with respective fossa on the prootic (Fig. 5C). The presence of this sulcus, its connection to the prootic fossa, and its posterior end at the base of the processus interfenestralis, and thus near the recessus scalae tympani, provide further tentative evidence that the fossa indeed is associated to the soft tissues that form an enclosed fluid-flow system between the fenestra ovalis, cavum labyrinthicum, foramen perilymphatica, and recessus scalae tympani (e.g. Evers & Benson, 2019; Foth et al., 2019).

A large facet for the exoccipital spans over the posteromedial margin of the opisthotic (Fig. 5A). The facet extends posteriorly halfway along the paroccipital process, indicating that the exoccipital had an elongate posterodorsolateral process. The size of the exoccipitals as inferred from their opisthotic facets suggests that the recessus scalae tympani, which is posteriorly framed by the exoccipital, was a large element. The dorsal margin of the foramen jugulare anterius is

618 visible as a gentle notch in the opisthotic's margin with the brain cavity (Fig. 5A) and located
619 just anterior to the facet for the exoccipital.
620 The paroccipital process of the opisthotic is relatively flat dorsoventrally (Figs. 2F, 5A), as in
621 *Uluops uluops* (UCM 53971), and has a thin edge posterior to the articulation facet for the
622 exoccipital. The lateral surface of the process lies against the quadrate and both are dorsally
623 overlapped by the squamosal.
624
625 **Parabasisphenoid.** The parabasisphenoid of UMZC T1041 is completely preserved and contacts
626 the pterygoid, prootic, opisthotic, and basioccipital (Figs. 2B, 7). A contact with the exoccipital
627 is not preserved, but cannot be ruled out, as well as possible anterior contacts with the palatines
628 or the vomer. The parabasisphenoid of *Pleurosternon bullockii* is anteroposteriorly elongate and
629 mediolaterally narrow (Fig. 7). The ventrally exposed surface of the parabasisphenoid is vaguely
630 triangular, as the parabasisphenoid narrows anteriorly to the rostrum basisphenoidale. Although
631 the pterygoids are not in perfect articulation with the parabasisphenoid in UMZC T1041, it
632 seems that the ventral surface of the rostrum basisphenoidale was exposed ventrally, separating
633 the pterygoids and preventing them from having a midline contact (see also Evans & Kemp,
634 1975). Indication for this interpretation comes from anteroposterior grooves to either side of the
635 rostrum basisphenoidale (Fig. 7B), which we interpret to be the articular facets of the pterygoid.
636 The ventral surface of the parabasisphenoid between these facets is completely smooth, just as
637 the adjacent ventral surface of the pterygoids, further support the notion that this bone was
638 exposed. Conversely, parts of the parabasisphenoid that are overlapped by the pterygoid are
639 usually roughened by articular ridges in comparative taxa like *Uluops uluops* (UCM 53971). A
640 ventrally exposed rostrum basisphenoidale has also been described for *Glyptops ornatus*

(Gaffney, 1979a), but it remains unclear, though plausible, if the pterygoids are fully separated by the parabasisphenoid in both taxa.

At about half the length of the parabasisphenoid of UMZC T1041, the basipterygoid process projects laterally from the ventrolateral margin of the bone (Fig. 7B–C, E). Although it has been argued that the process on the lateral margin of the basisphenoid of UMZC T1041 does not constitute a basipterygoid process (Gaffney, 1979a; Sterli et al., 2010), we agree with the original identification of Evans & Kemp (1975) and later assessments of the structure (e.g., Rabi et al., 2013). The basipterygoid process is subdivided into a dorsal and a ventral flange by a deep sulcus for the cerebral artery (Fig. 7E), which is also the case in *Uluops uluops* (UCM 53971). The dorsal flange is likely homologous with the basipterygoid process of other turtles, as the carotid system extends ventrally to it. The cerebral artery canal of UMZC T1041 fully enters the parabasisphenoid just anterior to the basipterygoid process via the foramen posterius canalis carotici cerebralis (see also Sterli et al., 2010) and projects anteromedially through the bone (Fig. 7E). The dorsal flange of the basipterygoid process is larger, and inserts deeply into the respective facet on the pterygoid. Anterior to the foramen posterius canalis carotici cerebralis, there is a faint and narrow groove that extends along the ventrolateral surface of the rostrum basisphenoidale. This groove is herein not interpreted as a narrow canal for the palatine artery, as it is not mirrored in the pterygoid bone. Instead, the pterygoid would fill the groove when articulated tightly with the parabasisphenoid. Thus, we herein interpret the groove as the delimitation of the facet for the pterygoid (Fig. 7B, E). The palatine canal therefore appears to be absent in UMZC T1041.

A peculiar feature of the basicranium of UMZC T1041 is the presence of a posterior process jointly formed by the parabasisphenoid and pterygoid (Fig. 7B–C, E), which overlaps the ventral

surface of the basioccipital. The parabasisphenoid part of this process is larger and more distinct than the pterygoid part. In UMZC T1041, the ventral surface of the posterior parabasisphenoid processes is slightly raised, and forms a shallowly concave fossa between them. Additionally, the surface of the process is textured by a short ridge. Such parabasisphenoid processes are also present in *Glyptops ornatus* (Gaffney, 1979a) and *Uluops uluops* (UCM 53971), and could be a pleurosternid synapomorphy. Posterolaterally projecting processes of the parabasisphenoid are also present in some baenids, such as *Eubaena cephalica* (Rollot, Lyson & Joyce, 2018), but the baenid process has less external relief, and seems better integrated into a flat ventral surface of the basicranium. Similar structures are also found in helochelydrids, in which these are sometimes referred to as a secondarily pair of tubercula basioccipitale (Joyce, Sterli & Chapman, 2014). In helochelydrids, these anterior tubercula basioccipitale are predominantly formed by the pterygoids (*Naomichelys speciosa*: Joyce, Sterli & Chapman, 2014), or entirely formed by the pterygoids (*Helochelydra nopscai*: Joyce et al., 2011). Despite these differences in composition of the processes, the anterior tubercula basioccipitale of helochelydrids and the posterior parabasisphenoid processes of pleurosternids share (i) that the posterior margin between them is concave; (ii) that they are slightly raised and form a concavity medially between them; (iii) that they overlap the basioccipital; and (iv) that their surface is textured indicating soft tissue insertion. Thus, topological and anatomical arguments suggest the homology of the pleurosternid and helochelydrid processes, and possibly provide evidence for paracryptodiran affinities of helochelydrids (see also Joyce, 2017; Joyce & Anquetin, 2019). To highlight this possible homology, we follow Joyce, Sterli & Chapman (2014) by calling these processes (anterior) tubercula basioccipitale (Fig. 7).

686 The dorsal surface of the parabasisphenoid of UMZC T1041 is extremely similar to the same
687 surface in *Uluops uluops* (UCM 53971) and YPM 4717, a specimen referred to *Glyptops*
688 *plicatulus* (our *Glyptops ornatus*) by Gaffney (1979a) based on temporal and geographic
689 reasoning. It can be divided into a posterior, slightly cup-like region that holds parts of the brain,
690 and the rostrum basisphenoidale anteriorly (Fig. 7A). In the posterior region, the
691 parabasisphenoid is dorsoventrally thickest. The posterolateral margin of the parabasisphenoid is
692 dorsally expanded. This expansion, which is also present in *Uluops uluops* (UCM 53971), forms
693 the ventral margin of the hiatus acusticus (Fig. 7A) and contacts the processus interfenestralis of
694 the opisthotic posteriorly and the prootic anteriorly (Fig. 5D). The lateral margins of the
695 parabasisphenoid anterior to the hiatus acusticus margin are gently raised, so that the medial
696 space between is transversely concave (Fig. 7A). The concavity is interrupted posteriorly by a
697 shallow basis tuberculi basalis (Fig. 7A, D), which would presumably have continued posteriorly
698 onto the basioccipital, as seen in *Uluops uluops* (UCM 53971). Foramina for the abducens nerve
699 are present anterolaterally on the dorsal parabasisphenoid surface. The respective anterior
700 foramina exit on the anterior basisphenoid surface within the retractor bulbi pits ventral to the
701 clinoid processes. The clinoid processes at the anterolateral corner of the parabasisphenoid cup
702 are extremely short (Fig. 7A, D), as is also the case in *Uluops uluops* (UCM 53971). The dorsum
703 sellae between the clinoid processes of UMZC T1041 is not developed as a vertical wall, but also
704 not as a horizontal sheet that overlaps the sella turcica. Instead, the dorsum sellae is only a very
705 minor, shallow ridge (Evans & Kemp, 1975; Fig. 7D). Ventrally underneath the ridge, the
706 anterior surface of the parabasisphenoid slopes toward the rostrum basisphenoidale and sella
707 turcica. This anterior surface is gently depressed and a midline ridge is absent (Fig. 7D). The
708 lateral aspects of the anterior surface are delimited by short vertical ridges that extend from the

base of the clinoid process downwards. These ridges also define deep retractor bulbi pits directly ventral to the clinoid processes (Fig. 7D). The retractor bulbi pits are further accentuated dorsally by a horizontal ridge at the base of the clinoid process, which is the same in *Glyptops ornatus* (Gaffney, 1979a). In *Uluops uluops* (UCM 53971), the anterior surface of the parabasisphenoid varies from *Glyptops ornatus* and *Pleurosternon bullockii* in lacking distinct retractor bulbi pits and having a deeper anterior surface ventral to the dorsum sellae. The rostrum basisphenoidale of UMZC T1041 extends anteriorly as a mediolaterally narrow sheet of bone. Its lateral margins are dorsally upturned, so that the sella turcica is well defined as a deep fossa (Fig. 7A, D). In the posterior margin of the sella turcica, the paired foramina anterius canalis carotici cerebralis are situated in relatively close proximity to one another (Fig. 7D).

Stapes. The stapes are not preserved for UMZC T1041.

Carotid circulation and facial nerve. Unambiguous osteological correlates are present in UMZC T1041 for the cerebral artery, the (undivided) facial nerve, and both major distal branches of the facial nerve, which are the hyomandibular and vidian nerves. As there is no evidence for a palatine artery canal, the palatine artery is either absent, or uncovered by bone, but located in an unusual position.

As described above (see parabasisphenoid), the basipterygoid process of UMZC T1041 is subdivided into a dorsal and a ventral flange (Fig. 7B–C, E), between which the canal for the cerebral artery starts to pierce the parabasisphenoid (Fig. 7E). This region is ventrally exposed, as the parabasisphenoid and pterygoid form a window-like recess around the basipterygoid articulation. No canalis caroticus internus is present posterior to the position of the basipterygoid

process, so that the internal carotid artery is not embedded in bone (see also Sterli et al., 2010). As the ventral flange of the basipterygoid process is much smaller than the dorsal flange, the artery can enter the basicranium via the small fenestra between the pterygoid and parabasisphenoid. As the artery directly enters the parabasisphenoid in this position, we do not classify this opening within the basipterygoid articulation as a foramen posterius canalis carotici interni (as done in Evans & Kemp, 1975), but as the foramen posterius canalis carotici cerebralis (as in Sterli, 2010). The palatine artery canal, if present, would be expected to extend anteriorly between the pterygoid and parabasisphenoid from the position of the foramen posterius canalis carotici cerebralis. Gaffney (1979a) indicated the presence of such a canal for *Glyptops ornatus*, but this should be revisited, as he did not find the anterior foramen for the palatine artery canal and thus might have misidentified the foramen for the vidian canal. In UMZC T1041, no palatine artery canal can be discerned. The parabasisphenoid, which is slightly disarticulated from the left pterygoid and strongly so from the right one, shows a subtle and narrow groove, that extends from the foramen posterius canalis carotici cerebralis forward and could thus be a candidate structure for the palatine artery canal (Fig. 7B). However, when the pterygoid is articulated, the respective groove is ‘closed’ by bone of the pterygoid, so that the groove likely constitutes a pterygoid facet, rather than a tiny canalis caroticus palatinum. As the posterior course of the internal carotid artery prior to its ‘split’ is not embedded in bone, the absence of the palatine artery canal does not necessarily warrant concluding that the artery itself is absent. However, as there is no indication of an interpterygoid slit or similar opening through which the palatine artery could eventually enter the cranium in UMZC T1041 or related taxa with more completely preserved anterior palate regions, the most parsimonious explanation of the observed pattern indeed is the loss of the palatine artery. The loss of the palatine artery has also been inferred for

other paracryptodires (Gaffney, 1975a; Lipka et al., 2006), including baenids (Rollot, Lyson & Joyce, 2018). However, the absence does not seem universal, as *Uluops uluops* clearly shows a palatine artery canal (UCM 53971). A palatine artery canal has also been reported for *Dorsetochelys typocardium* by Anquetin and André (2020), but these authors do not describe the canal system in detail and it thus remains unclear if the proposed palatine artery canal foramen reported for *Dorsetochelys typocardium* is indeed that or pertains to the canal system of the vidian nerve. Indeed, the posterior entry of the palatine artery described by Anquetin and André (2020) resembles that of the vidian canal described herein for *Pleurosternon bullockii* by piercing the pterygoid. As the situation in *Dorsetochelys typocardium* demands clarification, ideally by means of CT scanning, we will not further comment on this taxon herein. The condition of *Uluops uluops* (UCM 53971) is very similar to that *Pleurosternon bullockii* by having the carotid canal enter within a bifurcated basipterygoid process, although the former also has a foramen for the palatine artery. Uluops uluops (UCM 53971) shows, that no part of its internal carotid artery up to the point of its division is embedded by bone. In *Arundelemys dardeni*, the internal carotid artery itself is also not encased anteriorly, the palatine artery is absent, and the entry of the cerebral artery canal lies within a shallow fossa between the parabasisphenoid and pterygoid. All these turtles differ from baenids, in which the anterior part of the internal carotid artery is concealed by bone. This embedding of the internal carotid artery in baenids extends posteriorly up to the intersection of the carotid artery system with the canalis pro ramo nervi vidiani (Rollot, Lyson & Joyce, 2018). On the other hand, similarities between baenids, *Pleurosternon bullockii*, and *Arundelemys dardeni* exist in their shared absence of a palatine artery. Thus, most paracryptodires show similarities to one another in their carotid artery

777 system, but lots of within-group variation exists that can probably only be better understood once
778 the phylogenetic relations of these turtles are better characterized.
779 The facial nerve of UMZC T1041 exits the braincase laterally through the canalis nervus
780 facialis, which extends from the fossa acustico-facialis through the prootic and into the canalis
781 cavernosus. The position of the geniculate ganglion can be inferred to be within the canalis
782 cavernosus for UMZC T1041, because direct osteological evidence for the course of the
783 hyomandibular and vidian nerves begin there: the prootic has a hyomandibular sulcus that
784 extends from the lateral facial nerve canal foramen posteriorly to the cavum acustico-jugulare
785 (Fig. 7B). The vidian nerve passes ventrally through the pterygoid via the canalis pro ramo nervi
786 vidiani, which exits just posterior to the pterygoid ridge that borders the area of the basipterygoid
787 articulation (Fig. 7C). In turtles with an embedding of the internal carotid artery, the canalis pro
788 ramo nervi vidiani usually leads from the canalis cavernosus into the internal carotid canal (e.g.
789 Gaffney, 1979b). In UMZC T1041, which lacks an internal carotid canal, the vidian nerve is thus
790 transmitted to the ventral surface of the basicranium. From here, it is inferred to pass between the
791 dorsal and ventral flanges of the basipterygoid process, together with the carotid artery. Within
792 the facet for the basipterygoid process, the vidian nerve then enters the canalis nervus vidianus,
793 which starts in the center of the facet and extends anteriorly through the pterygoid. This posterior
794 foramen for the vidian canal was interpreted as a foramen posterius canalis carotici palatinum by
795 Sterli et al. (2010). However, the canal extends through the pterygoid only, instead of passing
796 along the parabasisphenoid-pterygoid suture, and exits anterolaterally from the sulcus cavernosus
797 (Fig. 6B, C), instead within the sulcus itself. Thus, the course and exit foramen of the canal
798 conform to the expectations of a canalis nervus vidianus (Rollot, Lyson & Joyce, 2018).
799

DISCUSSION

Paracryptodiran monophyly. The fossil turtle clade Paracryptodira was initially proposed based on the anterior position of the foramen posterius canalis carotici interni halfway along the contact of the basisphenoid with the pterygoid, in contrast to pleurodires, which have an entry that involved the prootic and/or quadrate, and crown cryptodires, which have an entry towards the posterior margin of the pterygoid (Gaffney, 1975a). The accuracy and utility of this character has been debated ever since (e.g., Evans & Kemp, 1976; Gaffney, 1979a; Rieppel, 1980; Sterli et al., 2010; Rabi et al., 2013), but progress has been hampered by confusing terminology and conflicting observations.

Our study suggests that two distinct morphotypes are present among paracryptodires. Whereas an anteriorly positioned foramen posterius canalis carotici interni indeed seems to be present in *Compsemys victa* (UCM 53971) and *Eubaena cephalica* (Rollot, Lyson & Joyce, 2018), this foramen is not present in *Pleurosternon bullockii* (UMZC T1041) and *Uluops uluops* (UCM 53971), as the internal carotid artery is embedded in bone in these taxa. This difference was initially disguised by terminology used from the 1970s to early 2000s, as the foramen posterius canalis carotici cerebralis was addressed as the foramen posterius canalis carotici interni (Rabi et al., 2013). Homology can nevertheless be maintained, if the foramen posterius canalis carotici interni is conceptualized as the entry to a small pit at the basisphenoid/pterygoid suture from which the cerebral and palatine arteries penetrate the surrounding bones, as had been reported for several paracryptodires, including *Glyptops ornatus* (Gaffney, 1979) or *Pleurosternon bullockii* (Sterli et al., 2010), but we are here able to demonstrate that this character concept is at least inapplicable to the latter, as the palatal canal is absent.

The above-listed differences should not be used to dismiss the fact that the carotid system, in general, enters the skull in all known paracryptodires from below relatively far anteriorly at or near the basisphenoid/pterygoid suture. Indeed, as the exact vessels penetrating the skull could only rarely be assessed prior to the use of CT scanning technology, we suspect from personal experience (WGJ) that the paracryptodiran condition was conceptualized by most authors by reference to topology, not the exact vessels that enter the skull. This broadened character concept, however, still pertains to two unrelated morphological aspects: first, the anterior placement of the entry of the carotid system and, second, the presence of an extended basisphenoid-pterygoid contact. The (derived) presence and extent of the basisphenoid-pterygoid contact is addressed in current phylogenetic analyses by other characters (e.g. Joyce, 2007; Sterli, 2010; Anquetin, 2012; Zhou & Rabi, 2015; Evers & Benson, 2019), while the (primitive) anterior placement of the carotid system entry could be grouped with the condition seen in basal turtles. So, while these two morphological aspects combined indeed diagnose paracryptodires relative to most other turtles, they are redundant with existing characters. We therefore here further support recent phylogenetic analysis (e.g. Evers & Benson, 2019) by suggesting that the 'paracryptodiran condition' should not be utilized as a carotid arterial character.

Although the most important 'paracryptodiran' cranial character can thus be debunked, pleurosternids, baenids, and other potential paracryptodires share several features that could potentially support their monophyly. In addition to the sculpturing of the shell (present in early baenids; e.g. Gaffney, 1972; Joyce & Anquetin, 2019), baenids and pleurosternids share some gross resemblance in their maxilla-premaxilla morphology, including a relatively strongly curved labial margin of the maxilla and a notch in the median section of the labial ridge along the premaxilla (Gaffney, 1972). Additionally, the jugal is dorsally removed from posteriorly

continuing the labial ridge otherwise formed by the maxilla (Gaffney, 1972). These features are, however, not unique to paracryptodires, as they also appear in extant turtles with ecologies that are probably similar to those of paracryptodires, such as riverine geoemydids (e.g. Gaffney, 1979b). To critically assess potential new paracryptodiran synapomorphies, the skulls of early baenids, particularly *Trinitichelys hiatti*, should be re-described.

Paracryptodiran relationships. This contribution is part of a larger study that attempts to better resolve the internal and external relationships of paracryptodires, if monophyletic, through a better understanding of their anatomy. Although the novel observations we made herein will be processed in later contributions, we take the liberty of highlighting similarities that particularly intrigue us and that may have phylogenetic significance.

Irrespective of paracryptodiran monophyly, our description of *Pleurosternon bullockii* provides morphological evidence for the content of Pleurosternidae, based on instances of similarities of *Pleurosternon bullockii* with some other taxa. Although a re-description of *Glyptops ornatus* is warranted to fully appreciate its anatomy, it is clear from existing information (e.g. Gaffney 1979a) that this taxon is indeed very similar to *Pleurosternon bullockii*, both in terms of general skull form, and in more detailed anatomical aspects. For instance, *Pleurosternon bullockii* and *Glyptops ornatus* share the following features: small prefrontals; long anterior processes of the frontals that partially separated the nasals; a squamosal-parietal contact; dorsal position of the jugal above the level of the labial margin of the maxilla; and, among other similarities in the parabasisphenoid morphology, the presence of anterior tubercula basioccipitale, the presence of a basipterygoid process, and the presence of deep retractor bulbi pits. The same is generally true for *Dorsetochelys typocardium*, in particular

868 the jugal exclusion from the orbit (DORCM G.00023; *contra* Evans & Kemp 1976) and the
869 presence of anterior tubercula basioccipitale (DORCM G.00023; not discernible in Evans &
870 Kemp 1976). In both cases, these similarities are not surprising, given that more recent
871 phylogenetic hypotheses already highlight close relationships among these turtles (e.g. Pérez-
872 García, Royo-Torres & Cobos, 2015; Joyce & Rollot, in press).
873 Although the skull of *Uluops uluops* deviates in general aspects of its cranial shape, we note a
874 great number of similarities between this taxon and *Pleurosternon bullockii*. Although *Uluops*
875 *uluops* has so far not been considered a pleurosternid (e.g. Carpenter & Bakker, 1990; Lyson &
876 Joyce 2011, Pérez-García, Royo-Torres & Cobos, 2015; Joyce and Rollot, in press), our
877 comparisons indicate that it might be attributable to this clade. Among the features that are
878 shared between *Uluops uluops* and *Pleurosternon bullockii* are a squamosal-parietal contact
879 (possibly plesiomorphically present in baenids; Gaffney 1972); the exclusion of the prootic from
880 the trigeminal foramen by a posteroventral ramus of the parietal (also present in
881 thalassochelydians and sandownids; Anquetin, Püntener & Joyce, 2017; Evers & Joyce, 2020);
882 the presence of an extended sulcus palatino-pterygoideus formed in part by an enlarged septum
883 orbitotemporale (similar to pleurodires, but also present in some cryptodires; Gaffney, Tong &
884 Meylan, 2006); presence of a deep fossa in the roof of the sulcus palatino-pterygoideus (also in
885 pleurodires; Gaffney, Tong & Meylan, 2006); dorsal position of the jugal above the level of the
886 labial margin of the maxilla (also present in baenids; Gaffney 1972); the size and shape of the
887 quadratojugal; the presence of a small quadrate-supraoccipital contact (unclear in early baenids);
888 the complete surrounding of the fenestra ovalis by the prootic and opisthotic (absent in
889 *Arundelemys dardeni* [USNM 41614]; unclear in other early baenids); the presence of a
890 hyomandibular nerve sulcus in the posterior part all of the canalis cavernosus (unclear in early

baenids); the presence of anterior tubercula basioccipitale (shared also with helochelydrids, see below); the presence of a basipterygoid process that is laterally invaded by the cerebral artery (absent in baenids and *Compsemys victa*, but symplesiomorphic for turtles); and the general shape of the parabasisphenoid (see description for full details). Although some of these characters may prove to be more widespread among paracryptodires in particular or stem-turtles more generally, the number of similar features between *Pleurosternon bullockii* and *Uluops uluops* lend support to the hypothesis that the latter is a pleurosternid.

We here also document intriguing similarities between *Pleurosternon bullockii* and helochelydrids, particularly in the anterior tubercula basioccipitale of the parabasisphenoid, but also in other features, such as the exclusion of the jugal from the orbit (e.g. Joyce et al., 2011; Joyce, Sterli & Chapman, 2014; Joyce 2017). Helochelydrids should be integrated into phylogenies with a dense sampling of paracryptodires to test if they are more closely related than currently thought.

We also note the presence of some features in *Pleurosternon bullockii* that are possibly more widespread among crownward stem-turtles than previously recognized, and which can therefore possibly aid in better constraining the global position of pleurosternids. For instance, a pterygoid-basioccipital contact has previously not been recognized in pleurosternids. This feature, considered diagnostic for baenids (Joyce & Lyson, 2015), is present in *Pleurosternon bullockii* and *Uluops uluops* (as well as in compsemydids and helochelydrids). Although thus probably widely present among paracryptodires, this feature probably cannot serve as a paracryptodiran synapomorphy, as several other clades that have repeatedly been hypothesized to be crownward stem turtles (e.g. Joyce 2007), including thalassochelydians, protostegids, and some xinjiangchelyids, also possess a pterygoid-basioccipital contact (Brinkman et al., 2013;

914 Anquetin, Püntener & Joyce, 2017; Evers, Barrett & Benson, 2019). Conversely, we here
915 demonstrate that a purported thalassochelydian synapomorphy, the presence of a posteroventral
916 process of the parietal along the posterior margin of the trigeminal foramen (Anquetin, Püntener
917 & Joyce, 2017), is also present in *Pleurosternon bullockii* (and also *Uluops uluops*). The two
918 examples of the pterygoid-basioccipital contact and the presence of a posteroventral parietal
919 process are a nice demonstration of how alleged synapomorphies or diagnostic features of
920 relatively inclusive group can have a much wider distribution across phylogeny. This highlights
921 (i) the importance of detailed descriptive work to acknowledge the anatomical variation present
922 across several clades; and (ii) the importance of global phylogenetic approaches to the
923 classification of fossil-only turtle clades. The latter is because the character state distribution
924 outside the 'focal clade' has importance not only for inference of global phylogenetic
925 placements, but also has an effect on in-group relationships and the optimization and polarity of
926 characters (e.g. Kluge & Farris, 1969; Farris, 1972; Nixon & Carpenter, 1993). The distribution
927 of the pterygoid-basioccipital contact, for instance, indicates that rather than being a local baenid
928 synapomorphy, it possibly represents a synapomorphy of the clade that includes paracryptodires
929 but also other probable crownward stem-turtle clades (e.g. Evers & Benson, 2019) such as
930 xinjiangchelyids or thalassochelydians. On the other hand, studies focused on more inclusive
931 focal groups without a global phylogenetic perspective often sample characters that document
932 variation among the suspected clade members to a finer level of detail than done in most global
933 studies (e.g. Joyce & Lyson, 2011, for paracryptodires). We think that it is important to reconcile
934 the finer-level studies with global phylogenetic approaches to address questions such as: do
935 baenids and paracryptodires form a monophylum?; or what is the global position of these clades?
936 We hope that detailed anatomical studies such as the one presented here lead to the recognition

of new phylogenetic characters as well as the revision of those that have been used in the past, so that the outlined questions can be more comprehensively addressed in the future.

On a final note, we find that *Pleurosternon bullockii* shows some remarkable similarities with pleurodire turtles, particularly in the orbitotemporal region of the skull, as well as the external process of the pterygoid. However, the orbitotemporal region of most fossil turtles is not sufficiently described to draw meaningful comparisons from the literature alone. CT scans of several specimens available to us, such as the xinjiangchelyid *Annemys* sp. (IVPP V18106; specimen described in Brinkman et al. [2013]), the probable sandownid *Solnhofia parsonsi* (TM 4023; specimen described in Gaffney [1975b]) or the plesiochelyid *Plesiochelys planiceps* (OUMNH J1582; specimen described in Gaffney [1976]) show that a strong ventral ridge of the postorbital that would form the septum orbitotemporale and define a narrow sulcus palatino-pterygoideus is absent in these turtles. This indicates that the similarity observed between *Pleurosternon bullockii* and pleurodires in regard to the septum interorbitale and related sulcus palatino-pterygoideus is unique, and not more widespread across the turtle stem. Similarly, the pleurodire-reminiscent morphology of the external pterygoid process of *Pleurostenon bullockii* is not seen in other crownward stem-turtles: the vertical flange of the external process of the pterygoid of *Pleurosternon bullockii* is comparatively larger than that of plesiochelyids or *Annemys* sp. Although both the size of the vertical flange and its slight medial deflection at the dorsal margin in *Pleurosternon bullockii* establishes some similarity to the pterygoid trochlea of pleurodires, important differences remain. For instance, the surface of the vertical flange of the external pterygoid process is oriented parallel to the skull midline, and not posterolaterally inclined. Unfortunately, the morphology of the pterygoid trochlea is unknown for stem-pleurodires (De Lapparent de Broin, de la Fuente & Fernandez, 2007), but a gradual evolution of

960 the pterygoid adductor musculature system via a double-trochlea along the external pterygoid
961 process and the otic capsule has been proposed as a possible evolutionary scenario (e.g. Joyce,
962 2007). Although the presence of a double trochlea does not seem to provide biomechanical
963 advantages according to analytical studies (Ferreira et al., 2020), all hypotheses for the evolution
964 of the pleurodire trochlea invoke a size increase of the external pterygoid process and its lateral
965 surface as an initial step (e.g. Joyce, 2007; Joyce & Sterli, 2012; Ferreira et al., 2020). Although,
966 at this point in time, we do not hypothesize that pleurosternids are stem-pleurodires, the
967 similarities noted herein should be further explored by additional comparisons and phylogenetic
968 implementation.
969
970 **CONCLUSIONS**
971 The cranial anatomy of *Pleurostenon bullockii* and comparative descriptions confirm high levels
972 of similarity with other hypothesized pleurosternids, such as *Glyptops ornatus* or *Dorsetochelys*
973 *typocardium*. Additionally, we note a large number of similarities between *Pleurosternon*
974 *bullockii* and *Uluops uluops*, which possibly is a pleurosternid as well. Among other features,
975 these taxa share a similar basipterygoid region, with the symplesiomorphic retention of a
976 basipterygoid process and a ventrally unimbedded internal carotid artery course, shared with
977 earlier diverging stem-turtles. These features, along with a relatively extensive dorsal skull
978 coverage and weakly developed otic trochleae, support the hypothesis that pleurosternids are
979 globally positioned among an extended stem-lineage of turtles. Our anatomical description of
980 *Pleurosternon bullockii* provides tentative evidence for close relationships between
981 pleurosternids and helochelydrids, which share unusual posterior processes of the
982 parabasisphenoid that form a second set of (anterior) tuberculae basioccipitale.

Although variation regarding the internal carotid region of the cranium exists among pleurosternids, it is clear that the anterior position of the foramen posterius canalis carotici interni, historically used as a synapomorphy to unite baenids and pleurosternids as Paracryptodira, is not present in pleurosternids, and results from misinterpretation of the respective anatomy. As other paracryptodiran cranial synapomorphies are also dubious, our observations challenge previous observations upon which traditional hypotheses regarding the systematics of paracryptodires were built. Although the monophyly of paracryptodires is thus currently not supported by evidence from cranial anatomy, CT documentation of early baenid cranial morphology is outstanding, and may provide such evidence in the future.

Pleurosternon bullockii shows a surprising number of similarities with pleurodires, which are seen in the area between the otic and temporal fossae. The formation of a relatively narrow sulcus palatino-pterygoideus by an expanded septum orbitotemporale is unparalleled in other crownward stem-turtles such as xinjiangchelyids or thalassochelydians. An expanded external pterygoid process with a dorsomedially deflected vertical flange also approaches the pleurodiran morphology. Further investigations are necessary to test if this morphology could be a model for an ancestral pleurodiran pterygoid trochlea.

INSTITUTIONAL ABBREVIATION

DORCM Dorset County Museum, Dorchester, United Kingdom.

IVPP Institute of Vertebrate Paleontology and Paleoanthropology, Chinese Academy of Sciences, Beijing, People's Republic of China.

OUMNH Oxford University Museum of Natural History, University of Oxford, Oxford, United Kingdom.

UCM Museum of Natural History, University of Colorado, Boulder, Colorado, USA.

UMZC Museum of Zoology, Cambridge University, Cambridge, United Kingdom.

USNM United States National Museum, Smithsonian Institution National Museum of Natural History, Washington, D.C., USA.

TM Teylers Museum, Haarlem, The Netherlands.

YPM Yale Peabody Museum of Natural History, New Haven, Connecticut, USA.

ACKNOWLEDGEMENTS

We thank Roger Benson (University of Oxford) for scanning the cranium of UMZC T1041 in our stead. Keturah Smithson is thanked for maintaining the scanner at the Cambridge Biotomography Center and Jason Head (University of Cambridge) is acknowledged for permission to study the specimen. The work is supported by a grant from the Swiss National Science Foundation (SNF 200021_178780/1).

REFERENCES

Anquetin J. 2012. Reassessment of the phylogenetic interrelationships of basal turtles (Testudinata). *Journal of Systematic Palaeontology* **10(1):**3–45.

Anquetin J, Püntener C, Billon-Bruyat J-P. 2015. *Portlandemys gracilis* n. sp., a new coastal marine turtle from the Late Jurassic of Porrentruy (Switzerland) and a reconsideration of plesiochelyid cranial anatomy. *PLoS ONE* **10(5):**e0129193.

Anquetin J, André C. 2020. The last surviving Thalassochelydia—a new turtle cranium from the Early Cretaceous of the Purbeck Group (Dorset, UK). *PaleorXiv*. doi:10.31233/osf.io/7pa5c.

1029 **Anquetin J, Püntener C, Joyce WG. 2017.** A review of the fossil record of turtles of the clade
1030 Thalassochelydia. *Bulletin of the Peabody Museum of Natural History* **58(2):**317–369.
1031 **Brinkman DB, Nicholls EL. 1993.** The skull of *Neurankylus eximius* (Testudines: Baenidae)
1032 and a reinterpretation of the relationships of this taxon. *Journal of Vertebrate Palaeontology*
1033 **13(3):**273–281.
1034 **Brinkman DB, Everth DA, Xu X, Clark JM, Wu X-C. 2013.** Turtles from the Jurassic
1035 Shishugou Formation of the Junggar Basin, People's Republic of China, with comments on
1036 the basicranial region of basal eucryptodires. In: Brinkman et al., eds. *Morphology and*
1037 *Evolution of Turtles*. Dordrecht: Springer Science+Buisness Media, 147–172.
1038 **Cadena EA, Parham JF. 2015.** Oldest known marine turtle? A new protostegid from the Lower
1039 Cretaceous of Colombia. *PaleoBios* **32:**1–42.
1040 **Carpenter K, Bakker RT. 1990.** A new latest Jurassic vertebrate fauna, from the highest levels
1041 of the Morrison Formation at Como Bluff, Wyoming. Part II. A new baenid turtle. *Hunteria*
1042 **2(6):**1–19.
1043 **De Lapparent de Broin F, de la Fuente MS, Fernandez MS. 2007.** *Notoemys laticentralis*
1044 (Chelonii, Pleurodira), Late Jurassic of Argentina: new examination of the anatomical
1045 structures and comparisons. *Revue de Paléobiologie* **26(1):**99–136.
1046 **Evans J, Kemp TS. 1975.** The cranial morphology of a new Lower Cretaceous turtle from
1047 Southern England. *Palaeontology* **18(1):**25–40.
1048 **Evans J, Kemp TS. 1976.** A new turtle skull from the Purbeckian of England and a note on the
1049 early dichotomies of cryptodire turtles. *Palaeontology*, 19**(2):**317–324.
1050 **Evers SW. 2020.** Project: Cranial CT scans of *Pleurosternon bullockii*. *MorphoSource*.
1051 Available at: https://www.morphosource.org/Detail/ProjectDetail/Show/project_id/1001

1052 **Evers SW, Benson RBJ. 2019.** A new phylogenetic hypothesis of turtles with implications for
1053 the timing and number of evolutionary transitions to marine lifestyles in the group.
1054 *Palaeontology* **62(1):**93–134.
1055 **Evers SW, Joyce WG. 2020.** A re-description of *Sandownia harrisi* (Testudinata: Sandownidae)
1056 from the Aptian of the Isle of Wight based on computed tomography scans. *Royal Society*
1057 *Open Science* **7:**191936.
1058 **Evers SW, Barrett PM, Benson RBJ. 2019.** Anatomy of *Rhinochelys pulchriceps*
1059 (Protostegidae) and marine adaptation during the early evolution of chelonioids. *PeerJ*
1060 **7:**e6811.
1061 **Evers SW, Neenan JM, Ferreira GS, Werneburg I, Barrett PM, Benson RBJ. 2019.**
1062 Neurovascular anatomy of the protostegid turtle *Rhinochelys pulchriceps* and comparisons of
1063 membranous and endosseous labyrinth shape in an extant turtle. *Zoological Journal of the*
1064 *Linnean Society* **187:**800–828.
1065 **Farris JS. 1972.** Estimating phylogenetic trees from distance matrices. *American Naturalist*
1066 **106:**645–668.
1067 **Ferreira GS, Lautenschlager S, Evers SW, Pfaff C, Kriwet J, Raselli I, Werneburg I. 2020.**
1068 Feeding biomechanics suggests progressive correlation of skull architecture and neck
1069 evolution in turtles. *Scientific Reports* **10:**5505.
1070 **Foth C, Evers SW, Joyce WG, Volpato V, Benson RBJ. 2019.** Comparative analysis of the
1071 shape and size of the middle ear cavity of turtles reveals no correlation with habitat ecology.
1072 *Journal of Anatomy* **235:**1078–1097.
1073 **Gaffney ES. 1972.** The systematics of the North American family Baenidae (Reptilia,
1074 Cryptodira). *Bulletin of the American Museum of Natural History* **147(5):**241–320.

1075 **Gaffney ES. 1975a.** A phylogeny and classification of the higher categories of turtles. *Bulletin*
1076 *of the American Museum of Natural History* **155(5):**387–436.
1077 **Gaffney ES. 1975b.** *Solnhofia parsonsi*, a new cryptodiran turtles from the Late Jurassic of
1078 Europe. *American Museum Novitates* **2576:**1–25.
1079 **Gaffney ES. 1976.** Cranial morphology of the European Jurassic turtles *Portlandemys* and
1080 *Plesiochelys*. *Bulletin of the American Museum of Natural History* **157(6):**487–544.
1081 **Gaffney ES. 1979a.** The Jurassic turtles of North America. *Bulletin of the American Museum of*
1082 *Natural History* **162(3):**91–136.
1083 **Gaffney ES. 1979b.** Comparative cranial morphology of Recent and fossil turtles. *Bulletin of the*
1084 *American Museum of Natural History* **164(2):**65–376.
1085 **Gaffney ES. 1990.** The comparative osteology of the Triassic turtle *Proganochelys*. *Bulletin of*
1086 *the American Museum of Natural History*, 19**4:**1–263
1087 **Gaffney ES. 1996.** The postcranial morphology of *Meiolania platyceps* and a review of the
1088 Meiolaniidae. *Bulletin of the American Museum of Natural History* **229:**1–166.
1089 **Gaffney ES, Meylan PA. 1988.** A phylogeny of turtles. In: Benton MJ, ed. *The Phylogeny and*
1090 *Classification of the Tetrapods, Volume 1: Amphibians, Reptiles, Birds, Systematics*
1091 *Association Special Volume 35A.* Oxford: Clarendon Press, 157–219.
1092 **Gaffney ES, Tong H, Meylan PA. 2006.** Evolution of the side-necked turtles: The families
1093 Bothremydidae, Euraxemydidae, and Araripemydidae. *Bulletin of the American Museum of*
1094 *Natural History* **300:**3–698.
1095 **Gaffney ES, Rich TH, Vickers-Rich P, Constantine A, Vacca R, Kool L. 2007.** *Chubutemys*,
1096 a new eucryptodiran turtles from the Early Cretaceous of Argentina, and the relationships of
1097 the Meiolaniidae. *American Museum Novitates* **3599:**1–35.

1098 **Joyce WG. 2007.** Phylogenetic relationships of Mesozoic turtles. *Bulletin of the Peabody*
1099 *Museum of Natural History* **48(1):**3–102.
1100 **Joyce WG. 2017.** A review of the fossil record of basal Mesozoic turtles. *Bulletin of the*
1101 *Peabody Museum of Natural History* **58(1):**65–113.
1102 **Joyce WG, Anquetin J. 2019.** A review of the fossil record of nonbaenid turtles of the clade
1103 Paracryptodira. *Bulletin of the Peabody Museum of Natural History* **60(2):**129–155.
1104 **Joyce WG, Lyson TR. 2015.** A review of the fossil record of turtles of the clade Baenidae.
1105 *Bulletin of the Peabody Museum of Natural History* **56(2):**147–183.
1106 **Joyce WG, Rollot Y. In Press.** An alternative interpretation of *Peltochelys duchastelii* as a
1107 paracryptodire. *Fossil Record*.
1108 **Joyce WG, Sterli J. 2012.** Congruence, non-homology, and the phylogeny of basal turtles. *Acta*
1109 *Zoologica* **93:**149–159.
1110 **Joyce WG, Chapman S, Moody RTJ, Walker CA. 2011.** The skull of the solemydid turtle
1111 *Helochelydra nopscai* from the Early Creatceous of the Isle of Wight (UK) and a review of
1112 Solemydidae. *Special Papers in Palaeontology* **86:**75–97.
1113 **Joyce WG, Sterli J, Chapman S. 2014.** The skeletal morphology of the solemydid turtle
1114 *Naomichelys speciosa* from the Early Cretaceous of Texas. *Journal of Paleontology*
1115 **88(6):**1257–1287.
1116 **Joyce WG, Rabi M, Clark JM, Xu X. 2016.** A toothed turtle from the Late Jurassic of China
1117 and the global biogeographic history of turtles. *BMC Evolutionary Biology* **16(236):**1–29.
1118 **Kluge AG, Farris JS. 1969.** Quantitative phyletics and the evolution of anurans. *Systematic*
1119 *Biology* **18:**1–32.

1120 **Lipka TR, Therrien F, Weishampel DB, Jamniczky HA, Joyce WG, Colbert MW,**
1121 **Brinkman DB. 2006.** A new turtle from the Arundel Clay Facies (Potomac Formation, Early
1122 Cretaceous) of Maryland, U.S.A. *Journal of Vertebrate Paleontology* **26(2):**300–307.
1123 **Lyson TR, Joyce WG. 2011.** Cranial anatomy and phylogenetic placement of the enigmatic
1124 turtle *Compsemys victa* Leidy, 1856. *Journal of Paleontology* **85(4):**749–801.
1125 **Milner AR. 2004.** The turtles of the Purbeck Limestone Group of Dorset, Southern England.
1126 *Palaeontology* **47(6):**1411–1467.
1127 **Nixon KC, Carpenter JM. 1993.** On outgroups. *Cladistics* **9:**413–426
1128 **Owen R. 1842.** Report on British fossil reptiles. Part II. In: *Report of the Eleventh Meeting of the*
1129 *British Association for the Advancement of Science; Held at Plymouth in July 1841.* London:
1130 Murray, 60–204.
1131 **Pérez-García A. 2014.** Revision of the poorly known *Dorsetochelys typocardium*, a relatively
1132 abundant pleurosternid turtle (Paracryptodira) in the Early Cretaceous of Europe. *Cretaceous*
1133 *Research* **49:**152–162.
1134 **Pérez-García A, Royo-Torres R, Cobos A. 2015.** A new European Late Jurassic pleurosternid
1135 (Testudines, Paracryptodira) and a new hypothesis of paracryptodiran phylogeny. *Journal of*
1136 *Systematic Palaeontology* **13(4):**351–369.
1137 **Rabi M, Zhou C-F, Wings O, Ge S, Joyce WG. 2013.** A new xinjiangchelyid turtle from the
1138 Middle Jurassic of Xinjiang, China and the evolution of the basipterygoid process in
1139 Mesozoic turtles. *BMC Evolutionary Biology* **13(203):**1–28.
1140 **Rabi M, Sukhanov VB, Egorova VN, Danilov I, Joyce WG. 2014.** Osteology, relationships,
1141 and ecology of *Annemys* (Testudines, Eucryptodira) from the Late Jurassic of Shar Teg,

1142 Mongolia, and phylogenetic definitions for Xinjiangchelyidae, Sinemydidae, and
1143 Macrobaenidae. *Journal of Vertebrate Paleontology* **34(2):**327–352.
1144 **Rieppel O. 1980.** The skull of the Upper Jurassic Cryptodire turtle *Thalassemys*, with a
1145 reconsideration of the chelonian braincase. *Palaeontographica, Abteilung A* 171:105–140.
1146 **Rollot Y, Lyson TR, Joyce WG. 2018.** A description of the skull of *Eubaena cephalica* (Hay,
1147 1904) and new insights into the cranial circulation and innervation of baenid turtles. *Journal*
1148 *of Vertebrate Paleontology* **38(3):**e1474886
1149 **Sterli J. 2010.** Phylogenetic relationships among extinct and extant turtles: the position of
1150 Pleurodira and the effects of fossils on rooting crown-group turtles. *Contributions to Zoology*
1151 **79(3):**93–106.
1152 **Sterli J, Müller J, Anquetin J, Hilger A. 2010.** The parabasisphenoid complex in Mesozoic
1153 turtles and the evolution of the testudinate basicranium. *Canadian Journal of Earth Sciences*
1154 **47:**1337–1346.
1155 **Sterli J, Pol D, Laurin M. 2013.** Incorporating phylgenetic uncertainty on phylogeny-based
1156 palaeontological dating and the timing of turtle diversification. *Cladistics* **29:**233–246.
1157 **Sukhanov VB. 2000.** Mesozoic turtles of middle and central Asia. In: Benton MJ, Shiskin MA,
1158 Unwin DM, Kurochkin EN, eds. *The Age of Dinosaurs in Russia and Mongolia.* Cambridge:
1159 Cambridge University Press, 309–367.
1160 **Zhou C-F, Rabi M. 2015.** A sinemydids turtle from the Jehol Biota provides insights into the
1161 basal divergence of crown turtles. *Scientific Reports* **5:**16299.
1162

Figure 1 Photographs of UMZC T1041, cranium of *Pleurosternon bullockii*. A, dorsal view. B, ventral view. C, left lateral view. D, right lateral view. E, anterior view. F, posterior view. Scale bar equals 10 mm.

Figure 2 Three dimensional renderings of the cranium of *Pleurosternon bullockii* (UMZC T1041). A, dorsal view. B, ventral view. C, left lateral view. D, right lateral view. E, anterior view. F, posterior view. Abbreviations: bsp, parabasisphenoid; ep, epipterygoid; f, frontal; j, jugal; mx, maxilla; n, nasal; op, opisthotic; pa, parietal; pmx, premaxilla; po, postorbital; pr, prootic; prf, prefrontal; pt, pterygoid; q, quadrate; qj, quadratojugal; soc, supraoccipital; sq, squamosal. Scale bars equal 10 mm.

Figure 3 Three dimensional renderings of the orbitotemporal region of *Pleurosternon bullockii* (UMZC T1041). A, anteroventral view of partial cranium. B, ventral view of partial cranium. Abbreviations: crcr, crista cranii; f, frontal; ftp, fossa temporalis; j, jugal; for, fossa orbitalis; pa, parietal; pip, processus inferior parietalis (descending process of parietal); po, postorbital; sol, sulcus olfactorius; sot, septum orbitotemporale; spp, sulcus palatino-pterygoideus. Scale bar equals 10 mm.

Figure 4 Three dimensional renderings of the trigeminal region of *Pleurosternon bullockii* (UMZC T1041). A, anterodorsolateral view of partial right cranium. B, anterolateral view of partial right cranium. Abbreviations: ep, epipterygoid; fnt, foramen nervi trigemini (trigeminal foramen); fst, foramen stapedio-temporale; pa, parietal; pepi, processus epipterygoideus; pip, processus inferior parietalis (descending process of parietal); pppa, posterior process of parietal

behind trigeminal foramen; pr, prootic; pt, pterygoid; pto-pr, prootic part of processus trochlearis oticum; pto-q, quadrate part of processus trochlearis oticum; q, quadrate; soc, supraoccipital. Scale bar equals 10 mm.

Figure 5 Three dimensional renderings of aspects of the cavum acustico-jugulare and the inner ear capsule of *Pleurosternon bullockii* (UMZC T1041). A, posteroventral view of partial right basicranium. B, posterolateral view of right prootic and pterygoid. C, lateral view of left prootic and opisthotic. D, medial view of left prootic and opisthotic. Abbreviations: acst, aditus canalis stapedio-temporalis; asc, anterior semicircular canal; bs-f, parabasisphenoid-facet; ccav, canalis cavernosus; ex-f, exoccipital facet; faf, fossa acustico-facialis; fja, foramen jugulare anterius; fnac, foramen nervi acustici; fov, fenestra ovalis; hac, hiatus acusticus; ica, incisura columella auris; lfng, lateral foramen nervi glossopharyngei; lsc, lateral semicircular canal; mfng, medial foramen nervi glossopharyngei; mfnf, medial foramen nervi facialis; op, opisthotic; pif, processus interfenestralis; plf, perilymphatic fossa; ppo, paroccipital process; pr, prootic; pr-lsc, prootic-part of the lateral semicircular canal; psc, posterior semicircular canal; pt, pterygoid; q, quadrate; snhy, sulcus nervi hyomandibularis; soc, supraoccipital. Scale bars equals 10 mm in A, 3 mm in B–D.

Figure 6 Three dimensional renderings of the right pterygoid of *Pleurosternon bullockii* (UMZC T1041). A, ventral view. B, dorsal view. C, anterodorsolateral view. Abbreviations: afnv, anterior foramen for the canalis nervus vidiani; bpp-f, basisptergyoid process facet; bsp-f, parabasisphenoid facet; ccav; canalis cavernosus; crpt, crista pterygoidei; ep-f, epipterygoid facet; j-f, jugal facet; mx-f, maxilla facet; pfnv, posterior foramen for the canalis nervus vidiani;

ppe, processus pterygoideus externus; pptp, posterior pterygoid process; pr-f, prootic facet; ptf, pterygoid fossa; q-f, quadrate facet; scav, sulcus cavernosus; vf, vertical flange of the external pterygoid process; vptr, ventral pterygoid ridge. Scale bar equals 3 mm.

Figure 7 Three dimensional renderings of the parabasisphenoid and basipterygoid process of *Pleurosternon bullockii* (UMZC T1041). A, parabasisphenoid in dorsal view. B, parabasisphenoid in ventral view. C, parabasisphenoid and left pterygoid in ventral view. D, parabasisphenoid in anterodorsal view. E, parabasisphenoid in left lateral and slight ventral view. Abbreviations: atbs, anterior tubercula basisphenoidale; bpp-df, dorsal flange of basipterygoid process; bpp-vf, ventral flange of basipterygoid process; cag, carotid groove; clp, clinoid process; cprnv, canalis pro ramo nervi vidiani; ctb, crista tuberculi basalis; ds, dorsum sellae; faccc, foramen anterius canalis carotici cerebralis; fna, foramen nervi abducentis; fpccc, foramen posterius canalis carotici cerebralis; pt-f, pterygoid facet; ptf, pterygoid fossa; rbp, retractor bulbi pit; rbs, rostrum basisphenoidale; st, sella turcica; vptr, ventral pterygoid ridge. Scale bar equals 3 mm.

Figure 1

Photographs of UMZC T1041, cranium of *Pleurosternon bullockii*.

A, dorsal view. B, ventral view. C, left lateral view. D, right lateral view. E, anterior view. F, posterior view. Scale bar equals 10 mm.

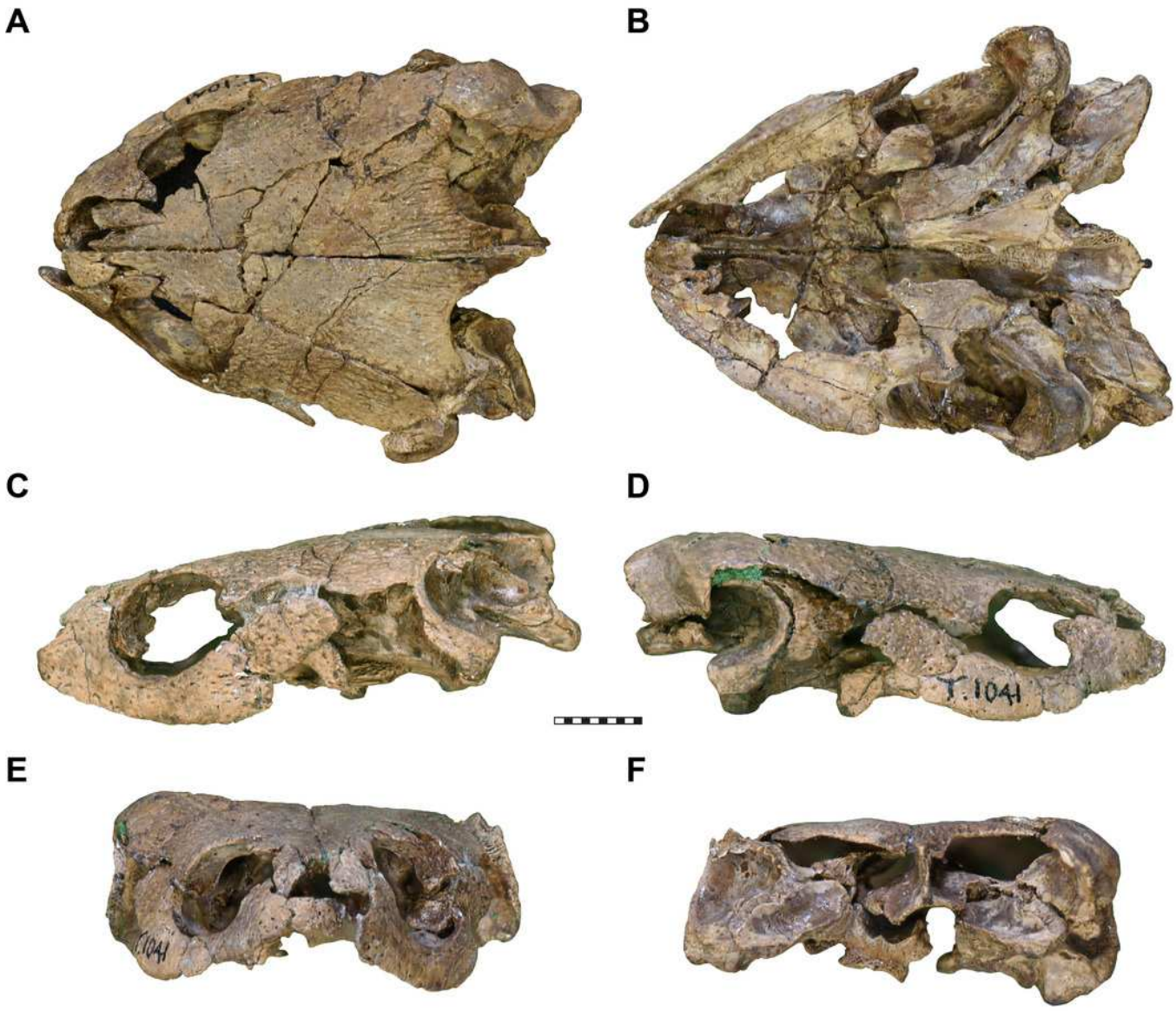

Figure 2

Three dimensional renderings of the cranium of *Pleurosternon bullockii* (UMZC T1041).

A, dorsal view. B, ventral view. C, left lateral view. D, right lateral view. E, anterior view. F, posterior view. Abbreviations: bsp, parabasisphenoid; ep, epipterygoid; f, frontal; j, jugal; mx, maxilla; n, nasal; op, opisthotic; pa, parietal; pmx, premaxilla; po, postorbital; pr, prootic; prf, prefrontal; pt, pterygoid; q, quadrate; qj, quadratojugal; soc, supraoccipital; sq, squamosal. Scale bars equal 10 mm.

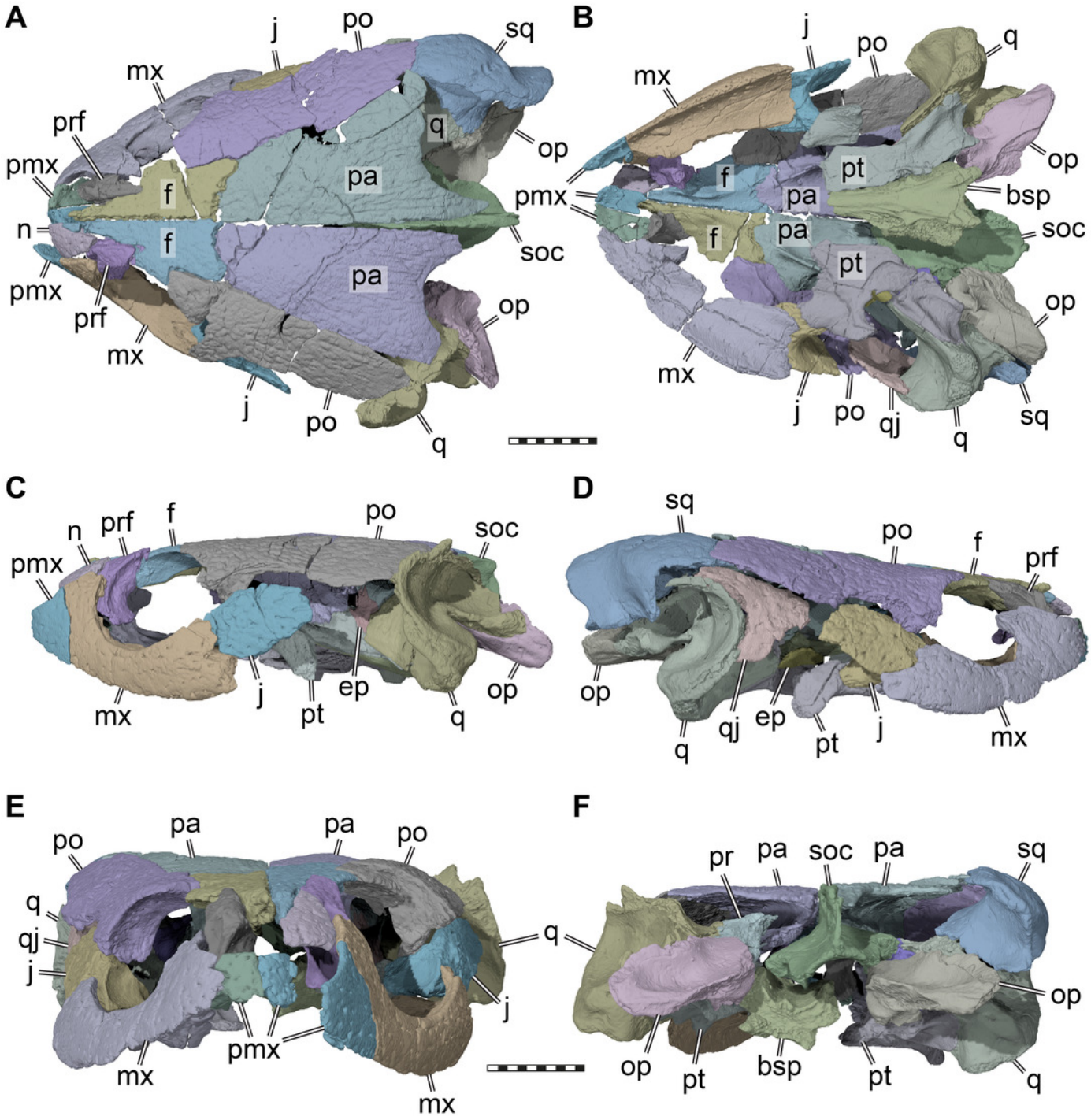
A
j
po
sq
mx
prf
q
op
pmx
pa
f
n
f
soc
pa
pmx
op
prf
mx
j
po
q
B
j
po
q
mx
op
pmx
f
pt
pa
bsp
f
pa
soc
pt
op
mx
j
po
qj
q
sq
C
n
prf
f
po
soc
pmx
mx
j
pt
ep
q
op
D
sq
po
f
prf
op
q
qj
ep
pt
j
mx
E
po
pa
pa
po
q
qj
j
q
j
mx
pmx
mx
F
pr
pa
soc
pa
sq
op
op
pt
bsp
pt
q

Figure 3

Three dimensional renderings of the orbitotemporal region of *Pleurosternon bullockii* (UMZC T1041).

A, anteroventral view of partial cranium. B, ventral view of partial cranium. Abbreviations: crcr, crista cranii; f, frontal; ftp, fossa temporalis; j, jugal; for, fossa orbitalis; pa, parietal; pip, processus inferior parietalis (descending process of parietal); po, postorbital; sol, sulcus olfactorius; sot, septum orbitotemporale; spp, sulcus palatino-pterygoideus. Scale bar equals 10 mm.

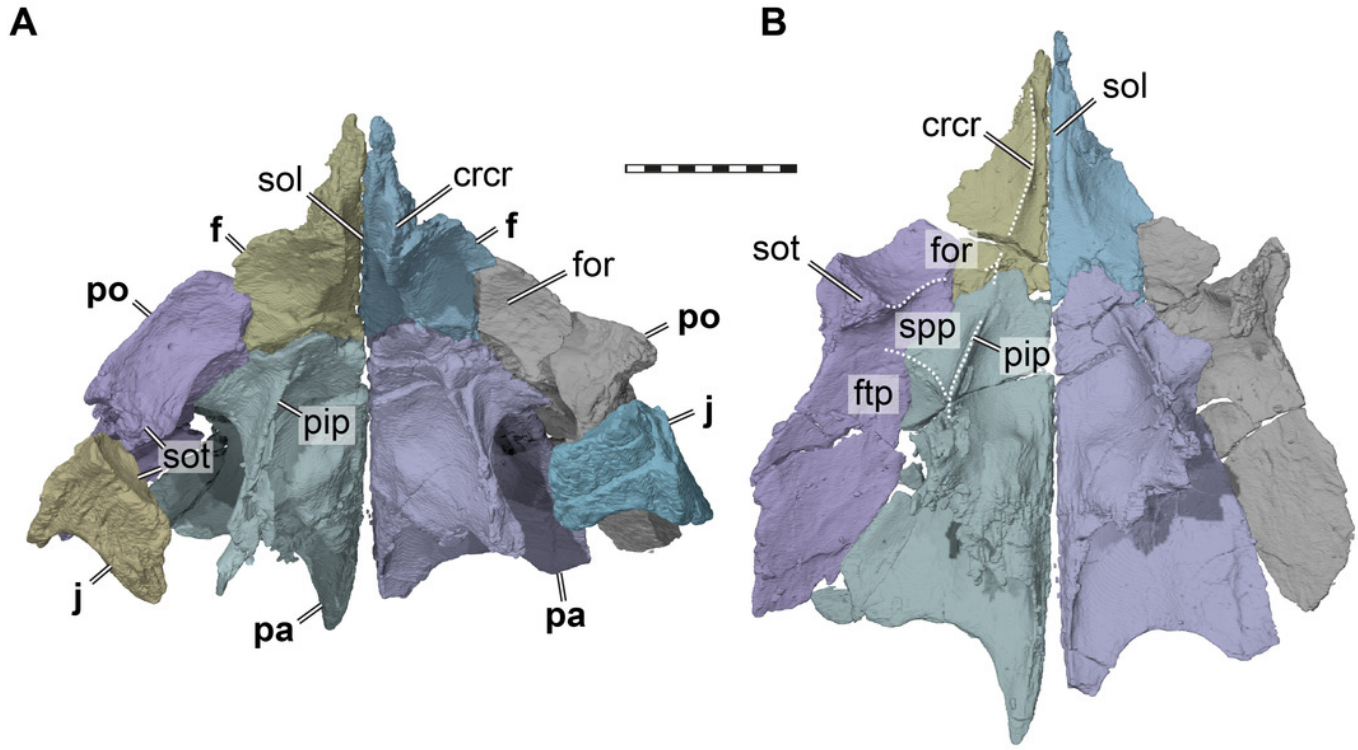

Figure 4

Three dimensional renderings of the trigeminal region of *Pleurosternon bullockii* (UMZC T1041).

A, anterodorsolateral view of partial right cranium. B, anterolateral view of partial right cranium. Abbreviations: ep, epipterygoid; fnt, foramen nervi trigemini (trigeminal foramen); fst, foramen stapedio-temporale; pa, parietal; pepi, processus epipterygoideus; pip, processus inferior parietalis (descending process of parietal); pppa, posterior process of parietal behind trigeminal foramen; pr, prootic; pt, pterygoid; pto-pr, prootic part of processus trochlearis oticum; pto-q, quadrate part of processus trochlearis oticum; q, quadrate; soc, supraoccipital. Scale bar equals 10 mm.

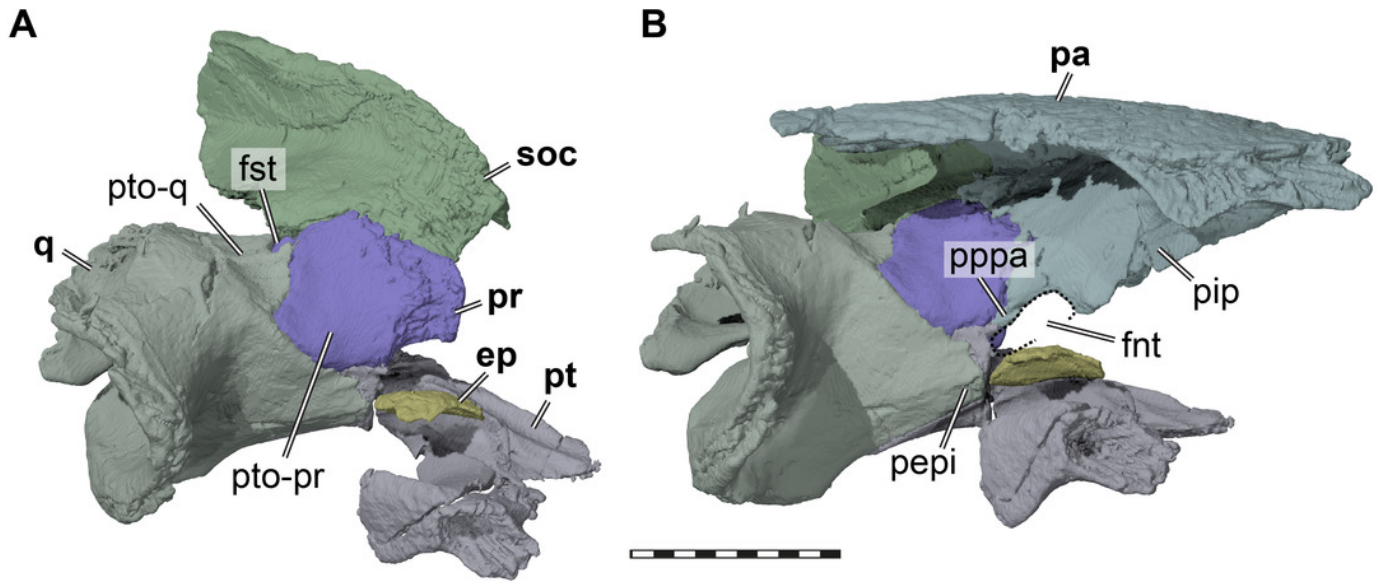

Figure 5

Three dimensional renderings of aspects of the cavum acustico-jugulare and the inner ear capsule of *Pleurosternon bullockii* (UMZC T1041).

A, posteroventral view of partial right basicranium. B, posterolateral view of right prootic and pterygoid. C, lateral view of left prootic and opisthotic. D, medial view of left prootic and opisthotic. Abbreviations: acst, aditus canalis stapedio-temporalis; asc, anterior semicircular canal; bs-f, parabasisphenoid-facet; ccav, canalis cavernosus; ex-f, exoccipital facet; faf, fossa acustico-facialis; fja, foramen jugulare anterius; fnac, foramen nervi acustici; fov, fenestra ovalis; hac, hiatus acusticus; ica, incisura columella auris; lfng, lateral foramen nervi glossopharyngei; lsc, lateral semicircular canal; mfng, medial foramen nervi glossopharyngei; mfnf, medial foramen nervi facialis; op, opisthotic; pif, processus interfenestralis; plf, perilymphatic fossa; ppo, paroccipital process; pr, prootic; pr-lsc, prootic-part of the lateral semicircular canal; psc, posterior semicircular canal; pt, pterygoid; q, quadrate; snhy, sulcus nervi hyomandibularis; soc, supraoccipital. Scale bars equals 10 mm in A, 3 mm in B–D.

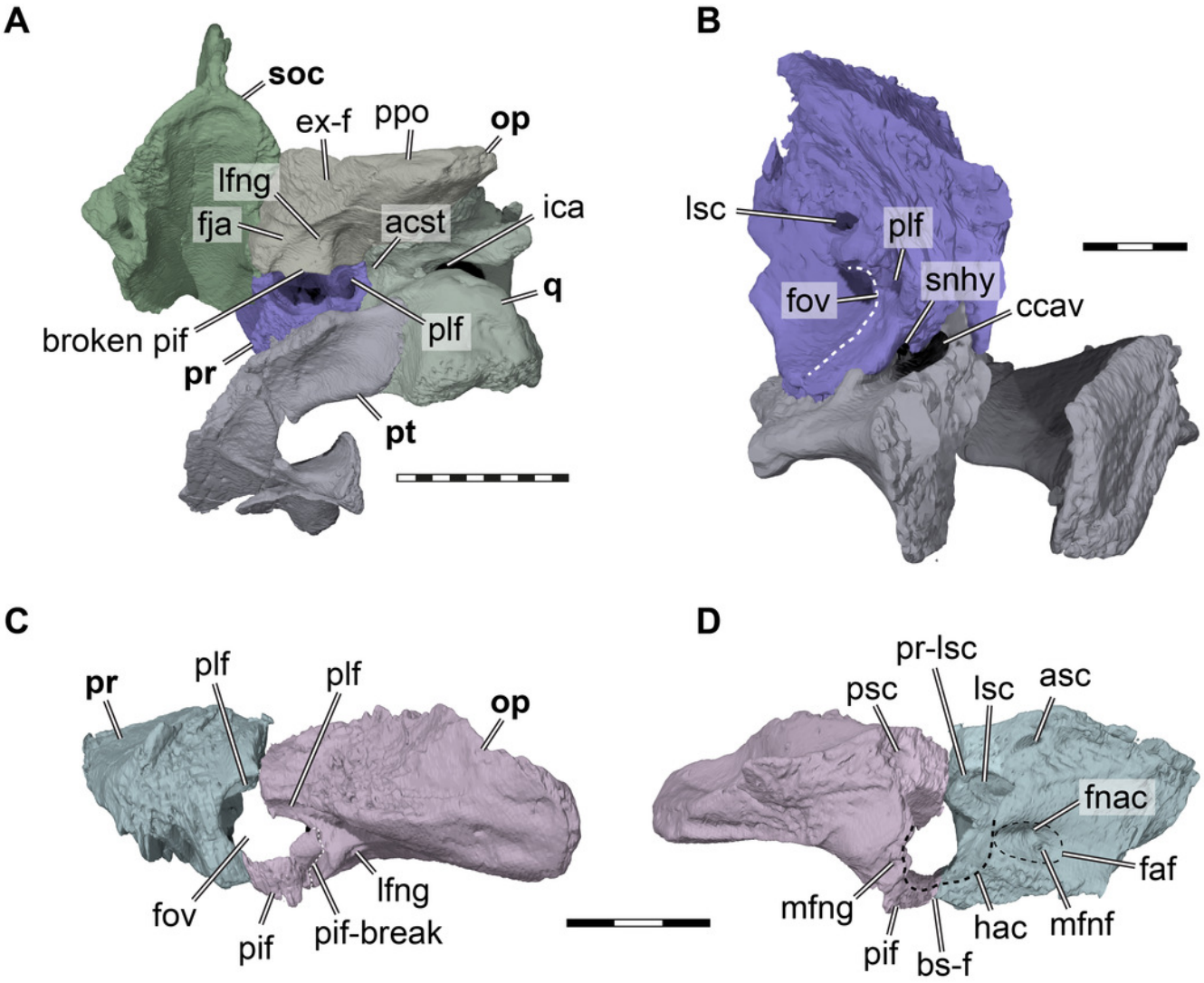
A
soc
ex-f
ppo
op
lfng
fja
acst
ica
q
broken pif
pr
plf
pt
B
lsc
plf
fov
snhy
ccav
C
pr
plf
plf
op
fov
pif
pif-break
lfng
D
pr-lsc
psc
lsc
asc
fnac
faf
mfng
pif
bs-f
hac
mfnf

Figure 6

Three dimensional renderings of the right pterygoid of *Pleurosternon bullockii* (UMZC T1041).

A, ventral view. B, dorsal view. C, anterodorsolateral view. Abbreviations: afnv, anterior foramen for the canalis nervus vidiani; bpp-f, basisptergyoid process facet; bsp-f, parabasisphenoid facet; ccav; canalis cavernosus; crpt, crista pterygoidei; ep-f, epipterygoid facet; j-f, jugal facet; mx-f, maxilla facet; pfnv, posterior foramen for the canalis nervus vidiani; ppe, processus pterygoideus externus; pptp, posterior pterygoid process; pr-f, prootic facet; ptf, pterygoid fossa; q-f, quadrate facet; scav, sulcus cavernosus; vf, vertical flange of the external pterygoid process; vptr, ventral pterygoid ridge. Scale bar equals 3 mm.

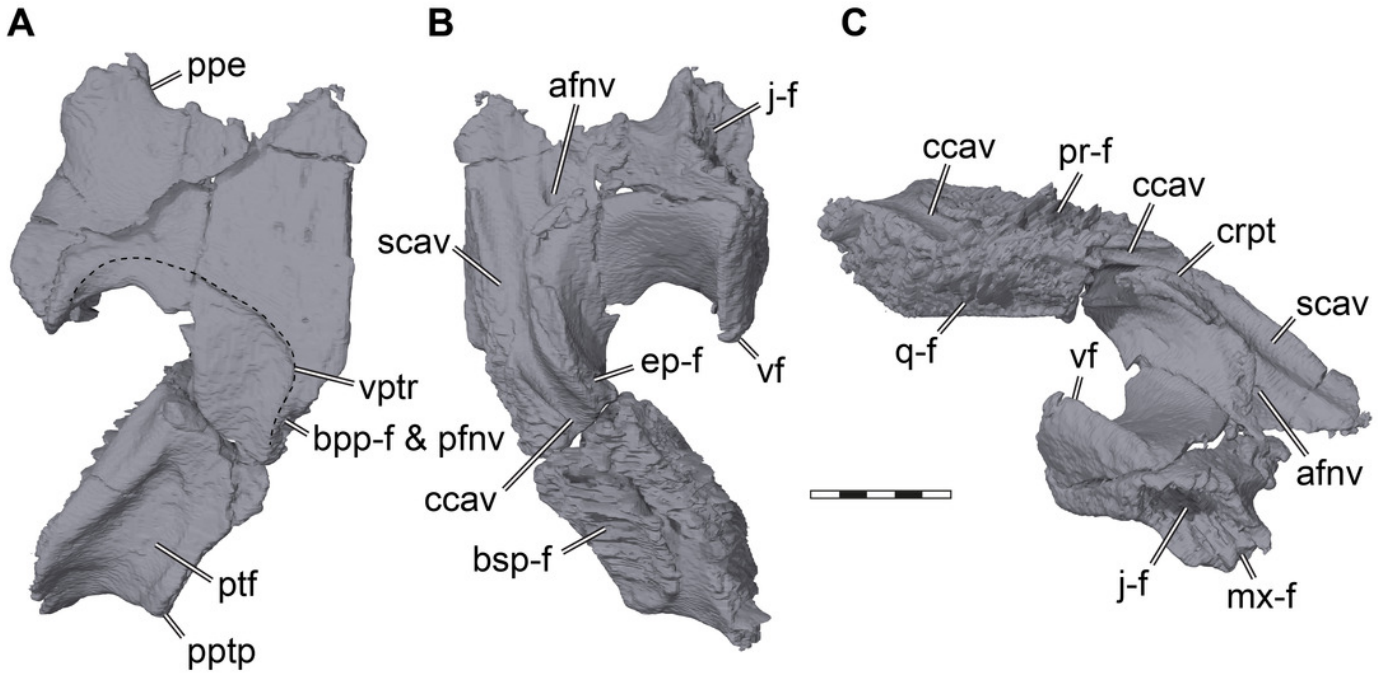

Figure 7

Three dimensional renderings of the parabasisphenoid and basipterygoid process of Pleurosternon bullockii (UMZC T1041).

A, parabasisphenoid in dorsal view. B, parabasisphenoid in ventral view. C, parabasisphenoid and left pterygoid in ventral view. D, parabasisphenoid in anterodorsal view. E, parabasisphenoid in left lateral and slight ventral view. Abbreviations: atbs, anterior tubercula basisphenoidale; bpp-df, dorsal flange of basipterygoid process; bpp-vf, ventral flange of basipterygoid process; cag, carotid groove; clp, clinoid process; ctb, crista tuberculi basalis; ds, dorsum sellae; faccc, foramen anterius canalis caroticus cerebralis; fna, foramen nervi abducentis; fpccc, foramen posterius canalis caroticus cerebralis; fprnv, foramen pro ramo nervi vidiani; pt-f, pterygoid facet; ptf, pterygoid fossa; rbp, retractor bulbi pit; rbs, rostrum basisphenoidale; st, sella turcica; vptr, ventral pterygoid ridge. Scale bar equals 3 mm.

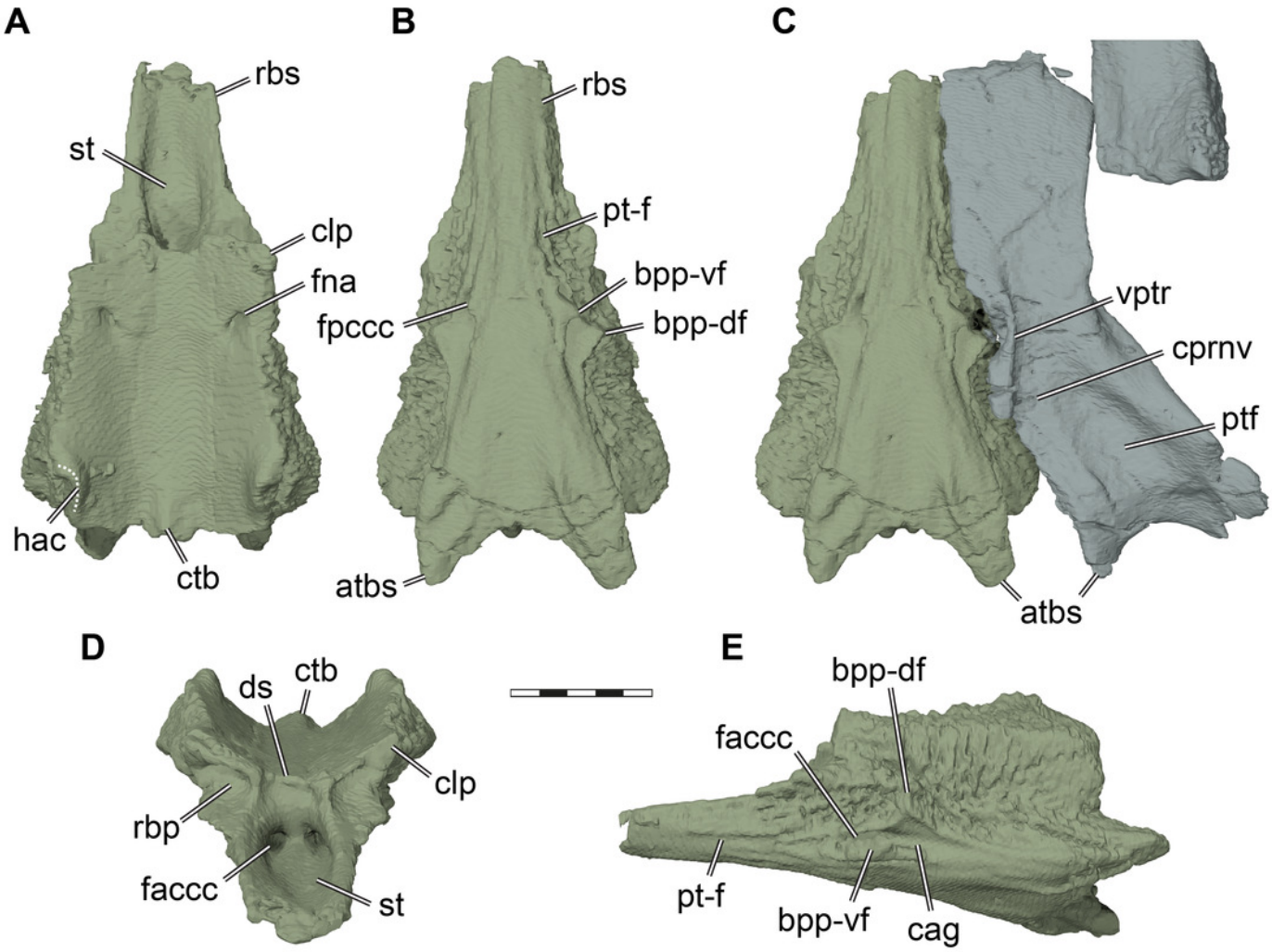
A
rbs
st
clp
fna
hac
ctb
B
rbs
pt-f
bpp-vf
fpccc
bpp-df
atbs
C
vptr
cprnv
ptf
atbs
D
ds
ctb
clp
rbp
faccc
st
E
bpp-df
faccc
pt-f
bpp-vf
cag